Supporting Information for

Low coordinate Zn(II) organocations bearing extremely bulky NHC ligands: structural features, air and water tolerance and use in hydrosilylation and hydrogenation catalysis.

Xuejuan Xu, Jordan Parmentier, Christophe Gourlaouen, Béatrice Jacques and Samuel Dagorne*

Institut de Chimie (UMR CNRS 7177), CNRS - Université de Strasbourg, 4, rue Blaise Pascal 67000 Strasbourg, France. Email : dagorne@unistra.fr

Table of Contents

1. NMR spectra of Zn complexes (Figs. S1-S24) pp. S2-S13

2. Crystallographical data (Fig. S25) p. S14

4. NMR spectra of the reactivity with H_2O of [**9**][$B(C_6F_5)_4$]) (Figs. S26-S31) pp. S15-S17

5. NMR spectra of the catalysis runs (Figs. S32-S36) pp. S18-S20

6. DFT calculation details, Lewis acidity and pKa estimations pp. S21-S22

7. References p. S23

NMR data of the Zn Complexes

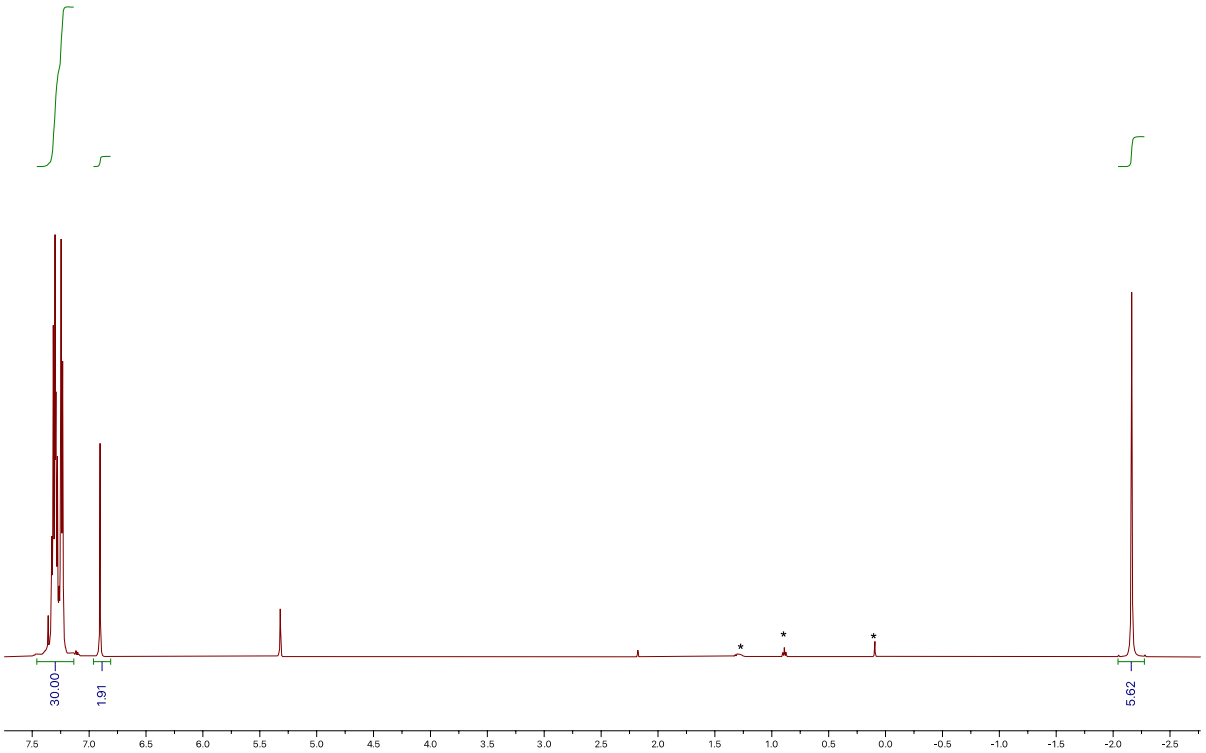

Figure S1. ^{1}H NMR (500 MHz) of $ITrZnMe_2$ (**1**) in CD_2Cl_2 (*: residual pentane and grease peaks).

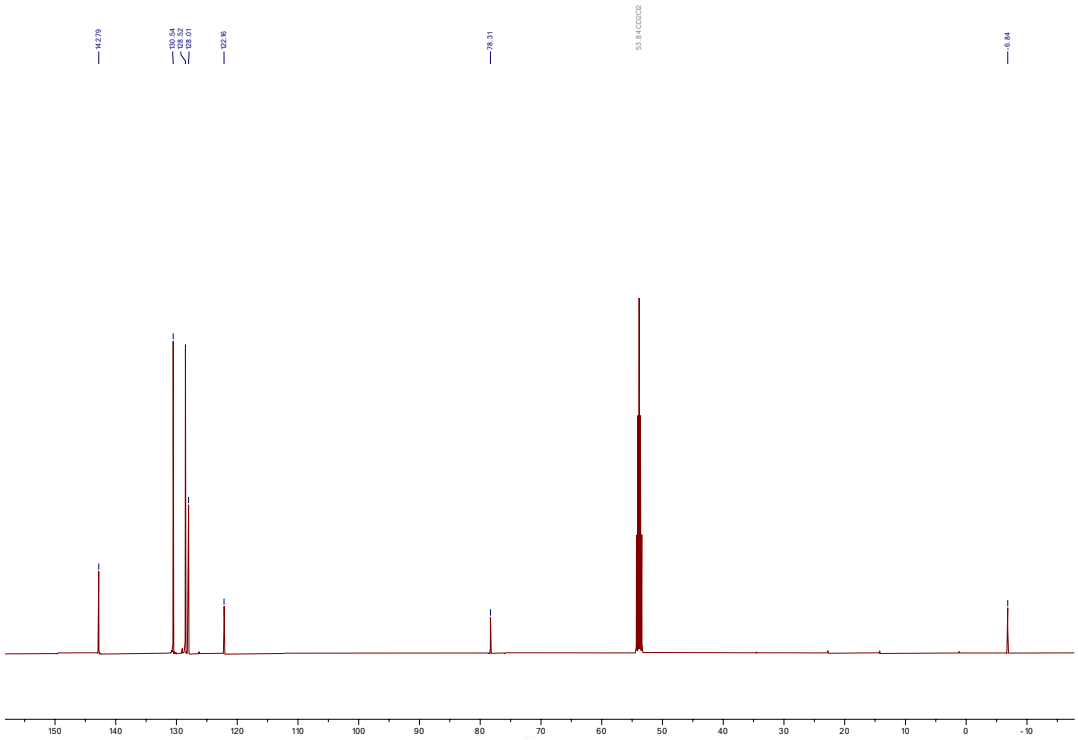

Figure S2. $^{13}C\{^{1}H\}$ NMR (125 MHz) of $ITrZnMe_2$ (**1**) in CD_2Cl_2.

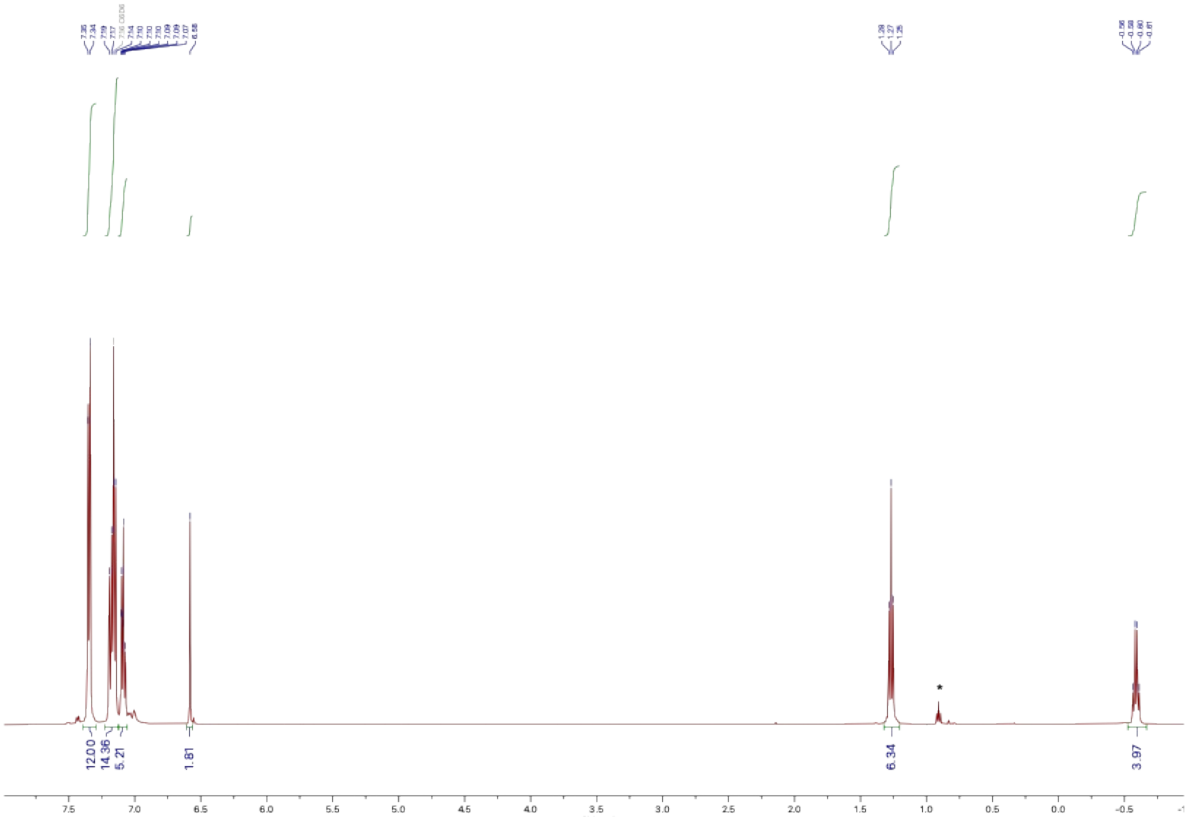

Figure S3. ^{1}H NMR (500 MHz) of $ITrZnEt_2$ (**2**) in C_6D_6 (*: residual pentane).

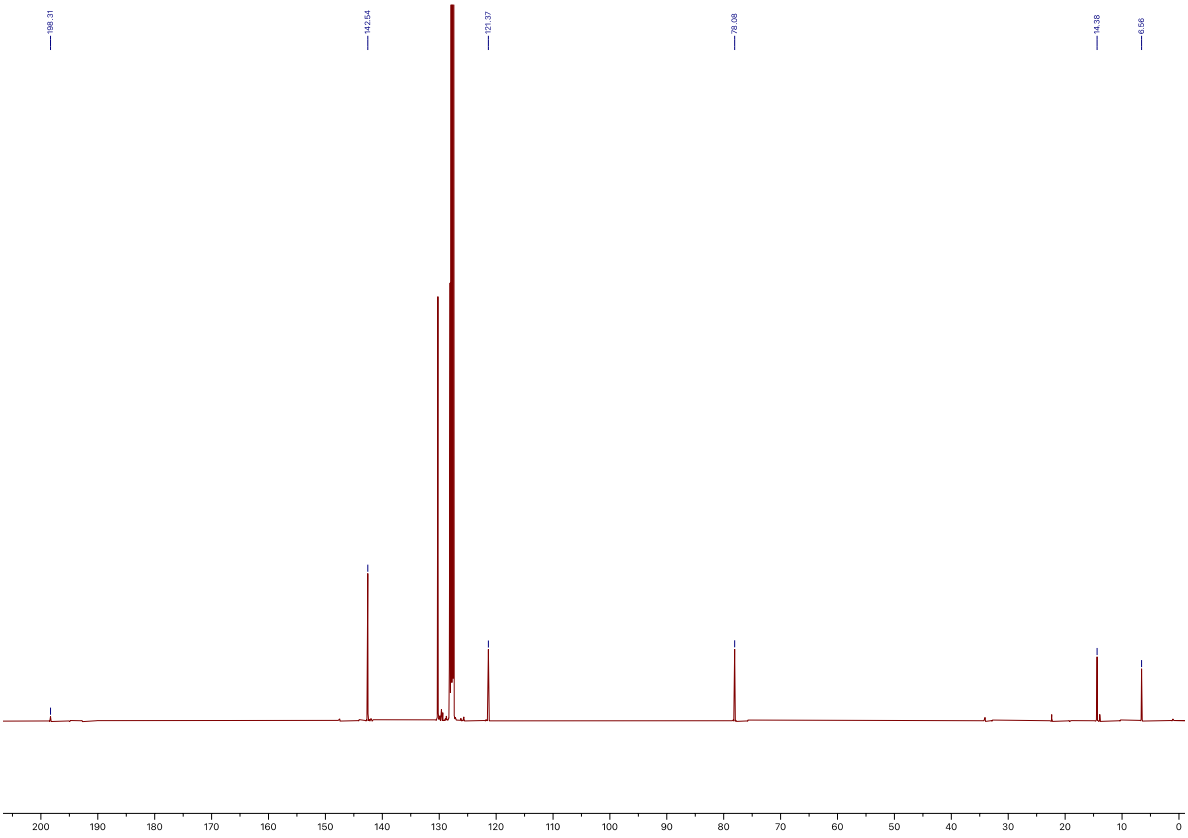

Figure S4. $^{13}C\{^{1}H\}$ NMR (125 MHz) of $ITrZnEt_2$ (**2**) in C_6D_6.

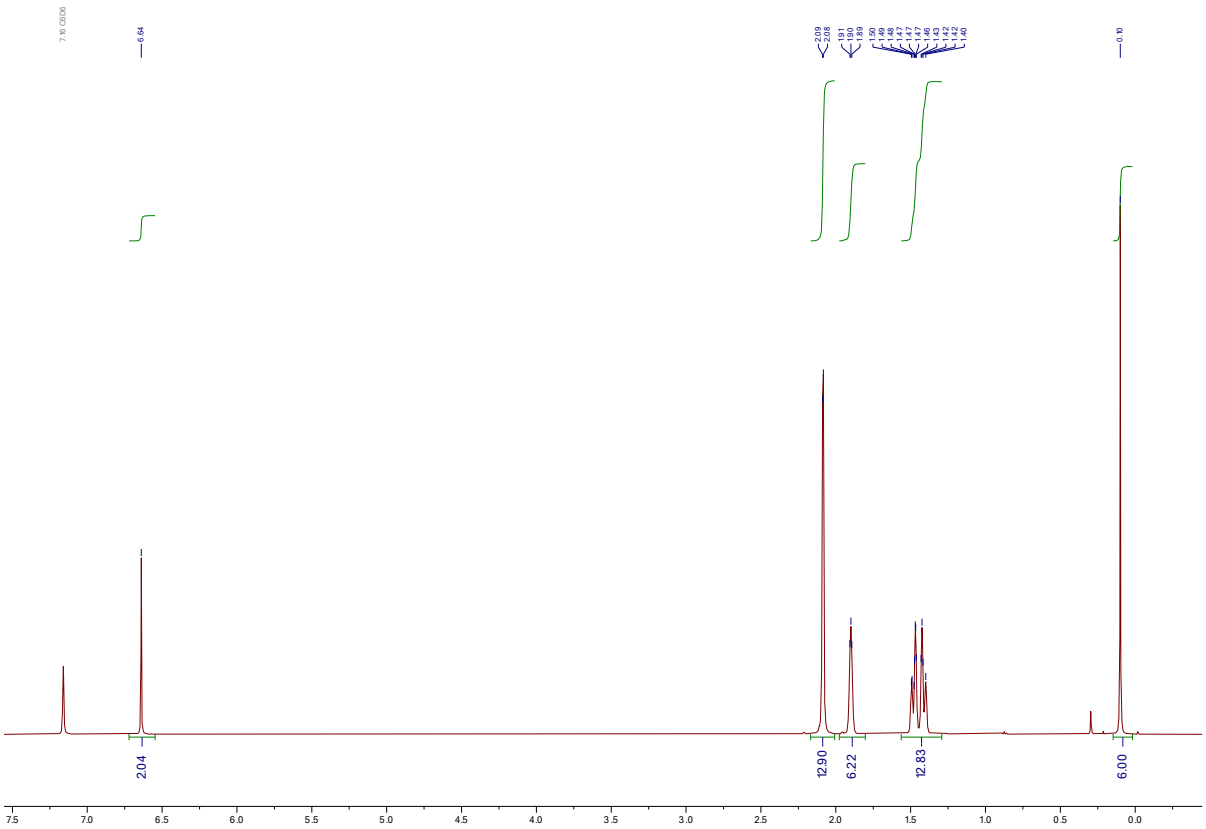

Figure S5. ^{1}H NMR (500 MHz) of IAdZnMe$_2$ (**3**) in C_6D_6.

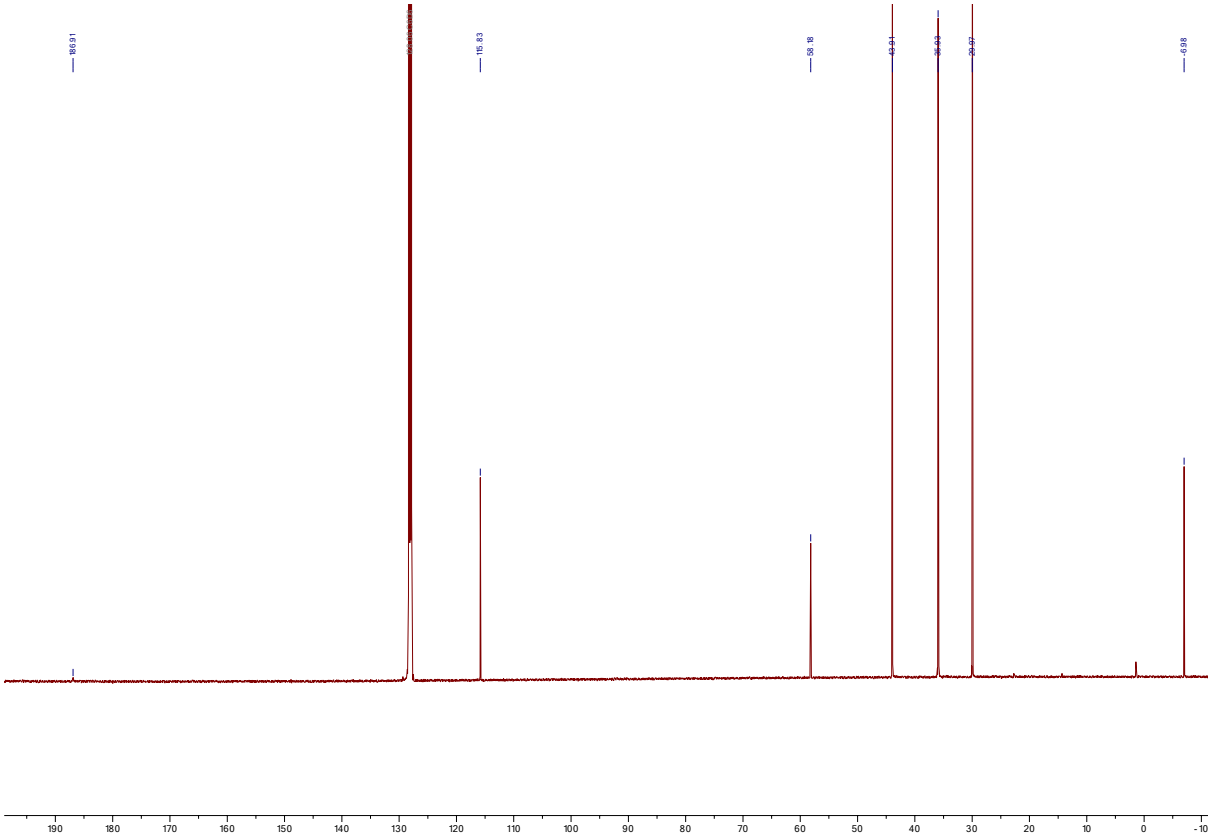

Figure S6. $^{13}C\{^{1}H\}$ NMR (125 MHz) of IAdZnMe$_2$ (**3**) in C_6D_6.

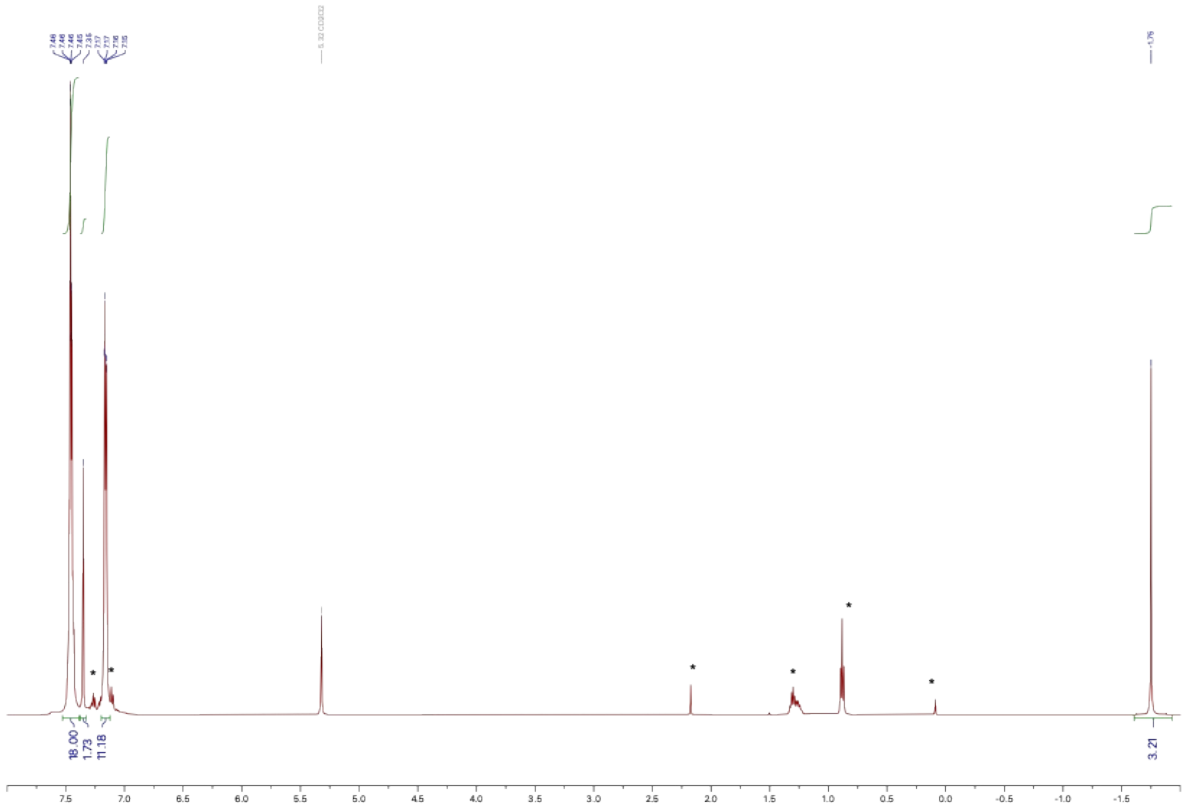

Figure S7. ^{1}H NMR (500 MHz) of [ITrZnMe][$B(C_6F_5)_4$] ([**5**][$B(C_6F_5)_4$]) in CD_2Cl_2 (*: residual solvent and grease peaks).

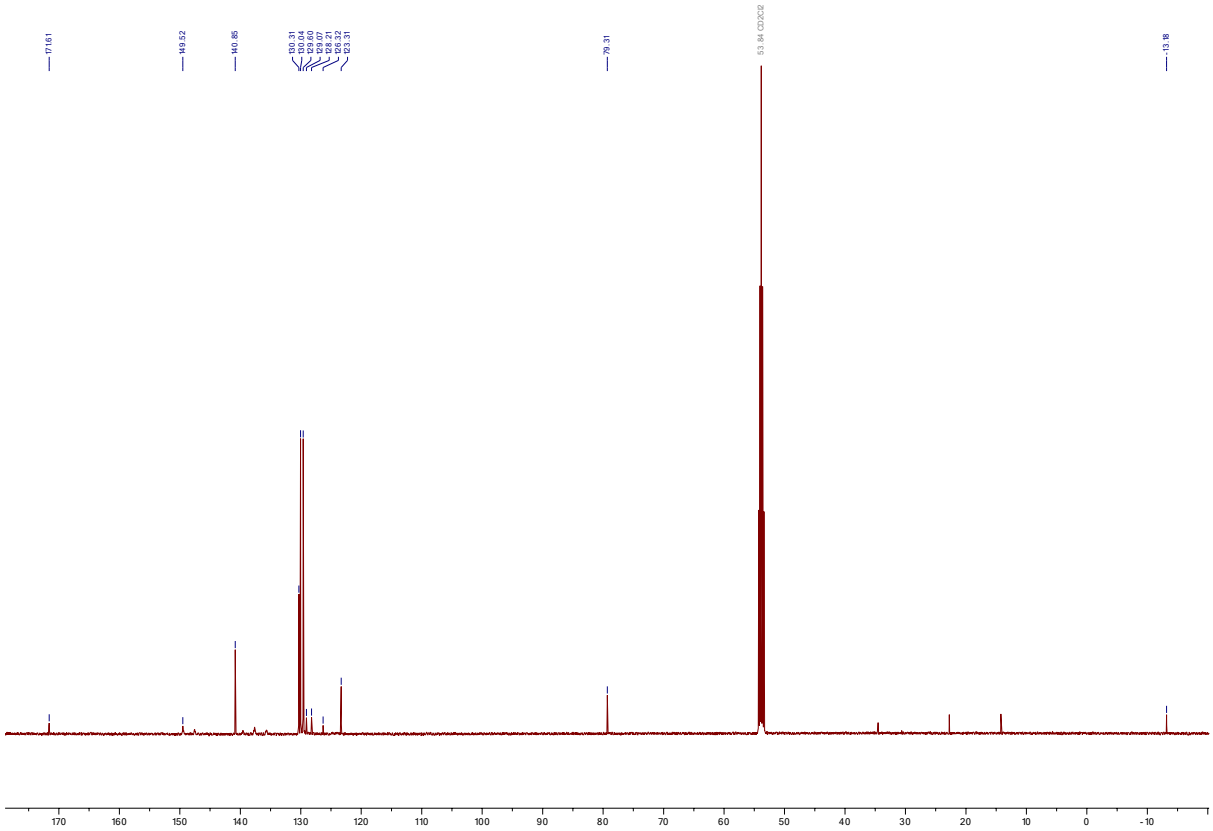

Figure S8. $^{13}C\{^{1}H\}$ NMR (125 MHz) of [ITrZnMe][$B(C_6F_5)_4$] ([**5**][$B(C_6F_5)_4$]) in CD_2Cl_2.

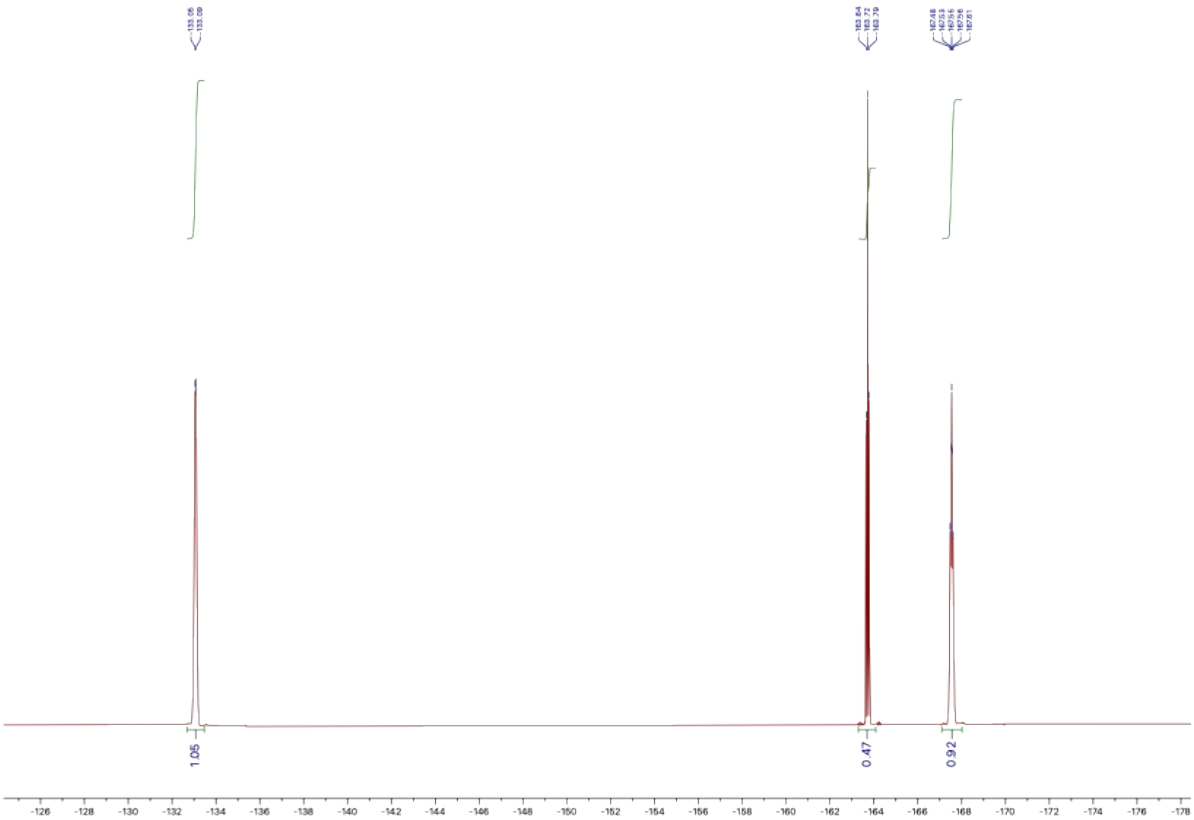

Figure S9. ^{19}F NMR (282 MHz) of [ITrZnMe][$B(C_6F_5)_4$] ([**5**][$B(C_6F_5)_4$]) in CD_2Cl_2.

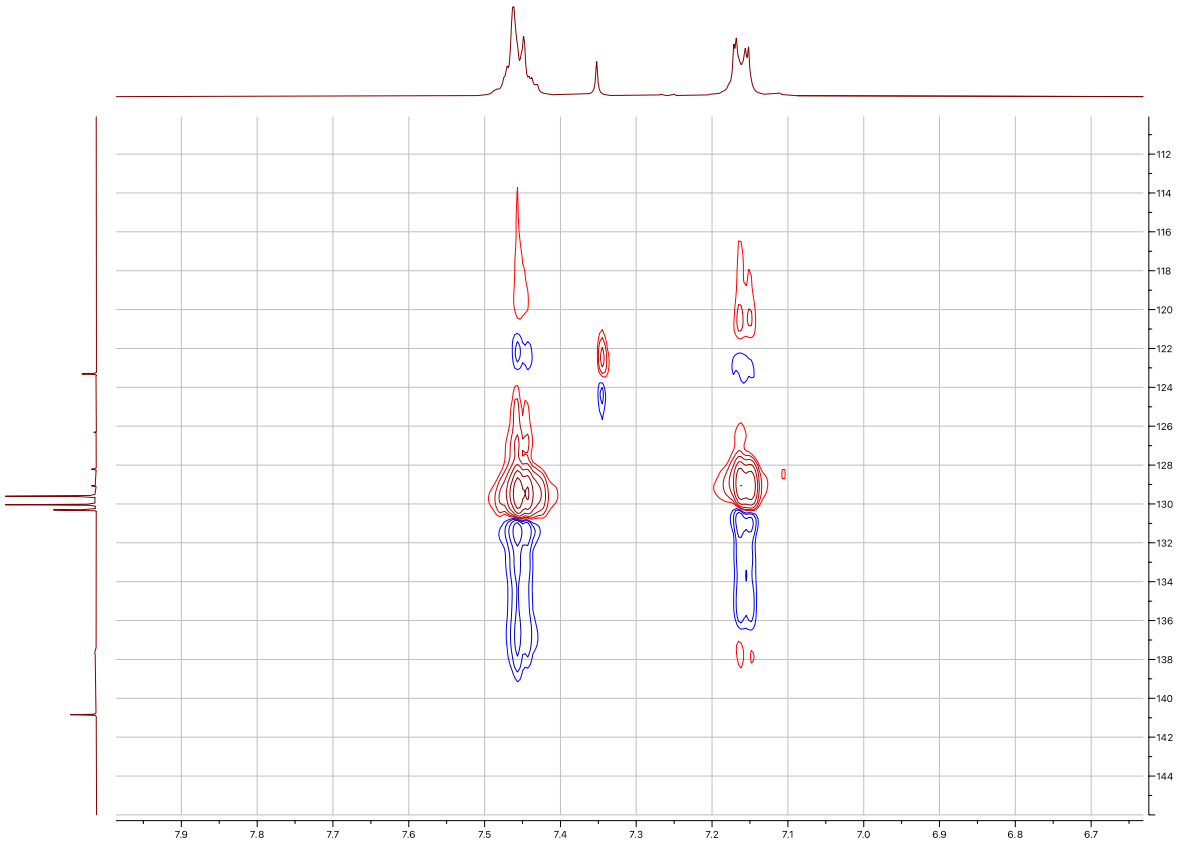

Figure S10. 2D HSQC NMR (500 MHz) of [ITrZnMe][$B(C_6F_5)_4$] ([**5**][$B(C_6F_5)_4$]) in CD_2Cl_2. Zoom-in on the aromatic region of the ^1H NMR data.

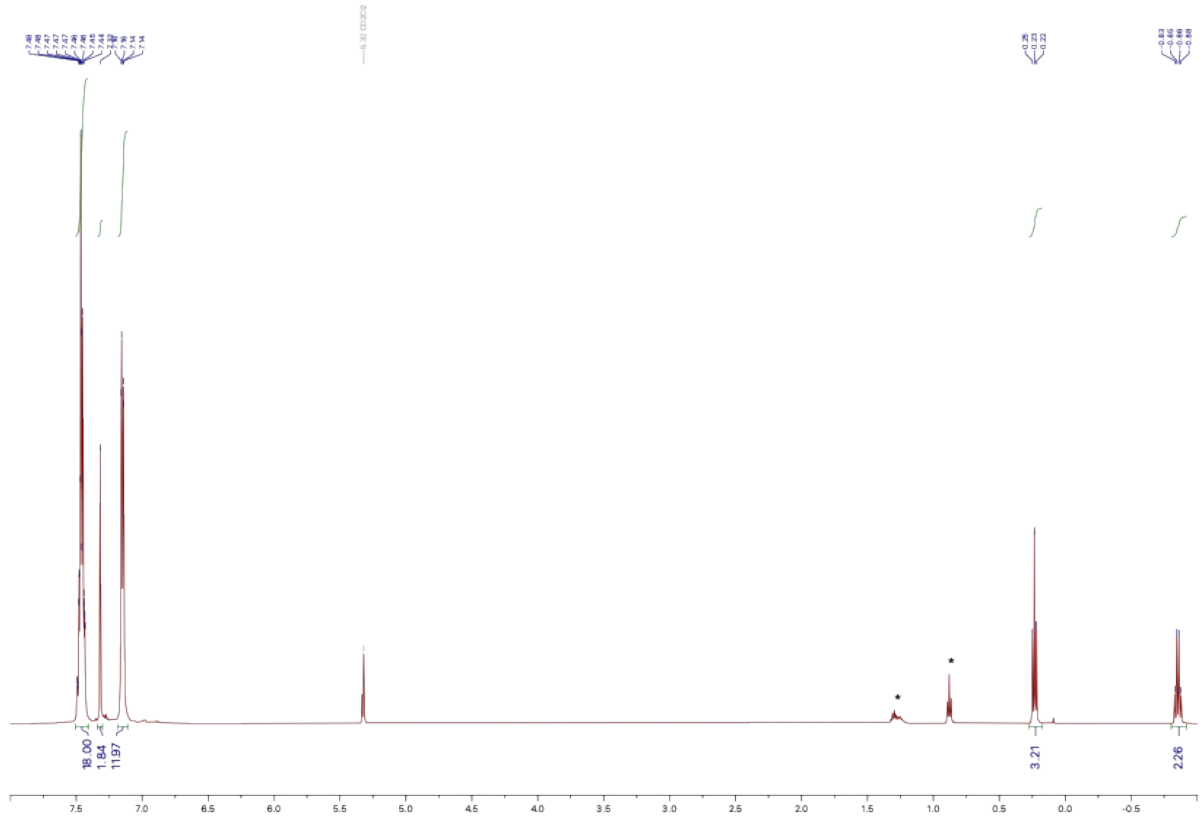

Figure S11. ^{1}H NMR (500 MHz) of [ITrZnEt][$B(C_6F_5)_4$] ([**6**][$B(C_6F_5)_4$]) in CD_2Cl_2 (*: residual pentane).

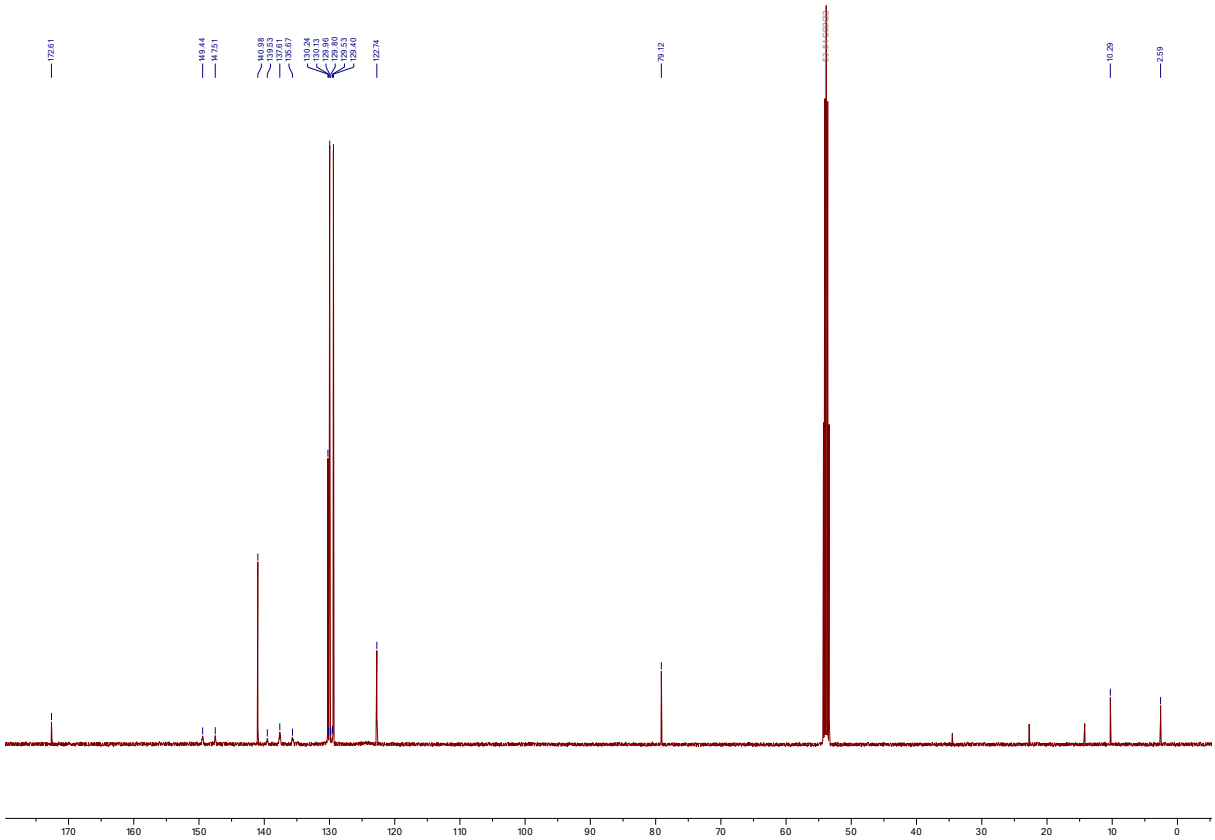

Figure S12. $^{13}C\{^{1}H\}$ NMR (125 MHz) of [ITrZnEt][$B(C_6F_5)_4$] ([**6**][$B(C_6F_5)_4$]) in CD_2Cl_2.

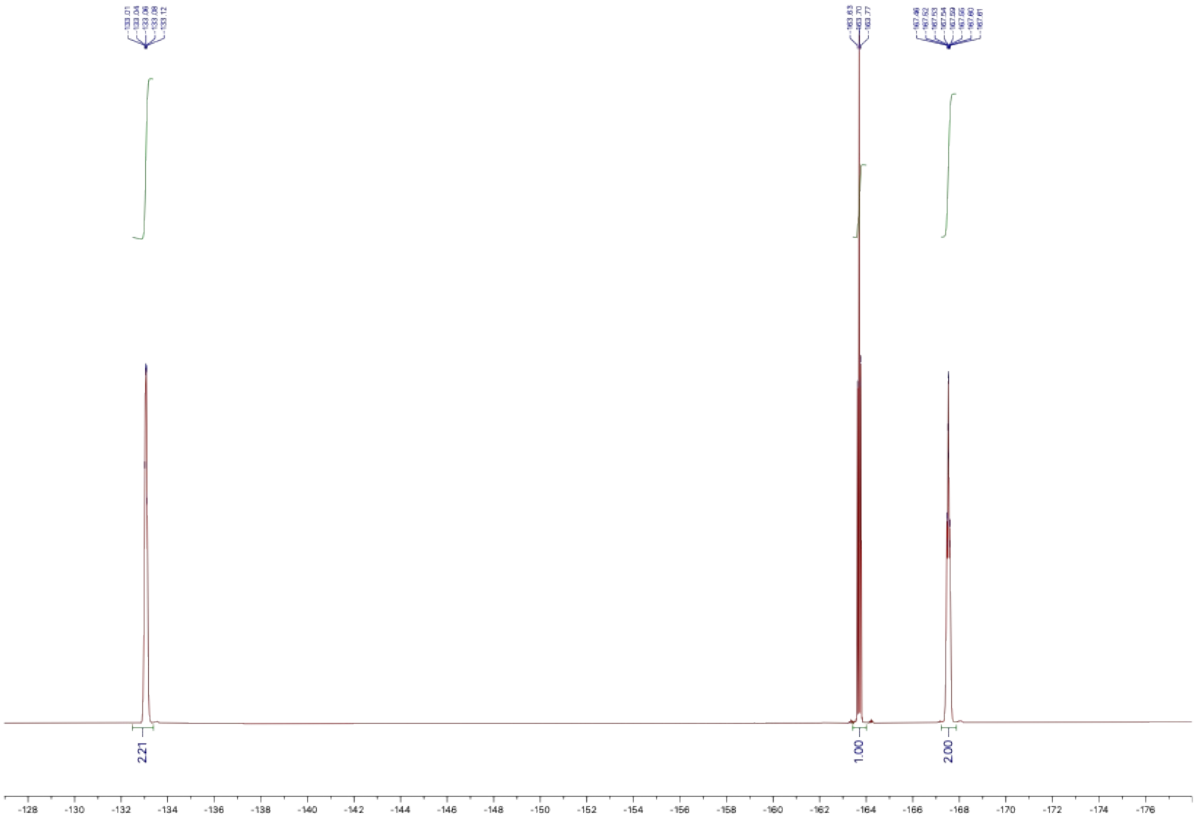

Figure S13. ^{19}F NMR (282 MHz) of [ITrZnEt][$B(C_6F_5)_4$] ([**6**][$B(C_6F_5)_4$]) in CD_2Cl_2.

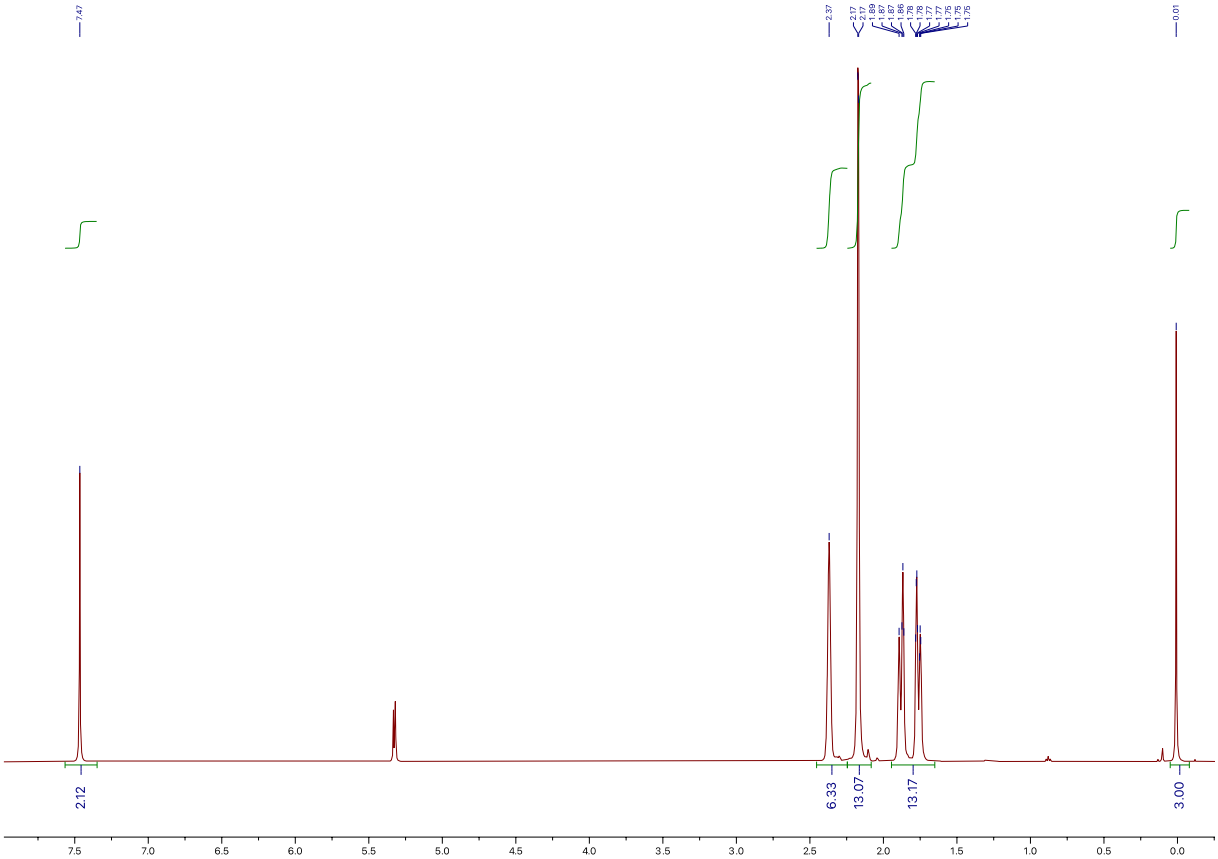

Figure S14. ^{1}H NMR (500 MHz) of [IAdZnMe][$B(C_6F_5)_4$] ([**7**][$B(C_6F_5)_4$]) in CD_2Cl_2.

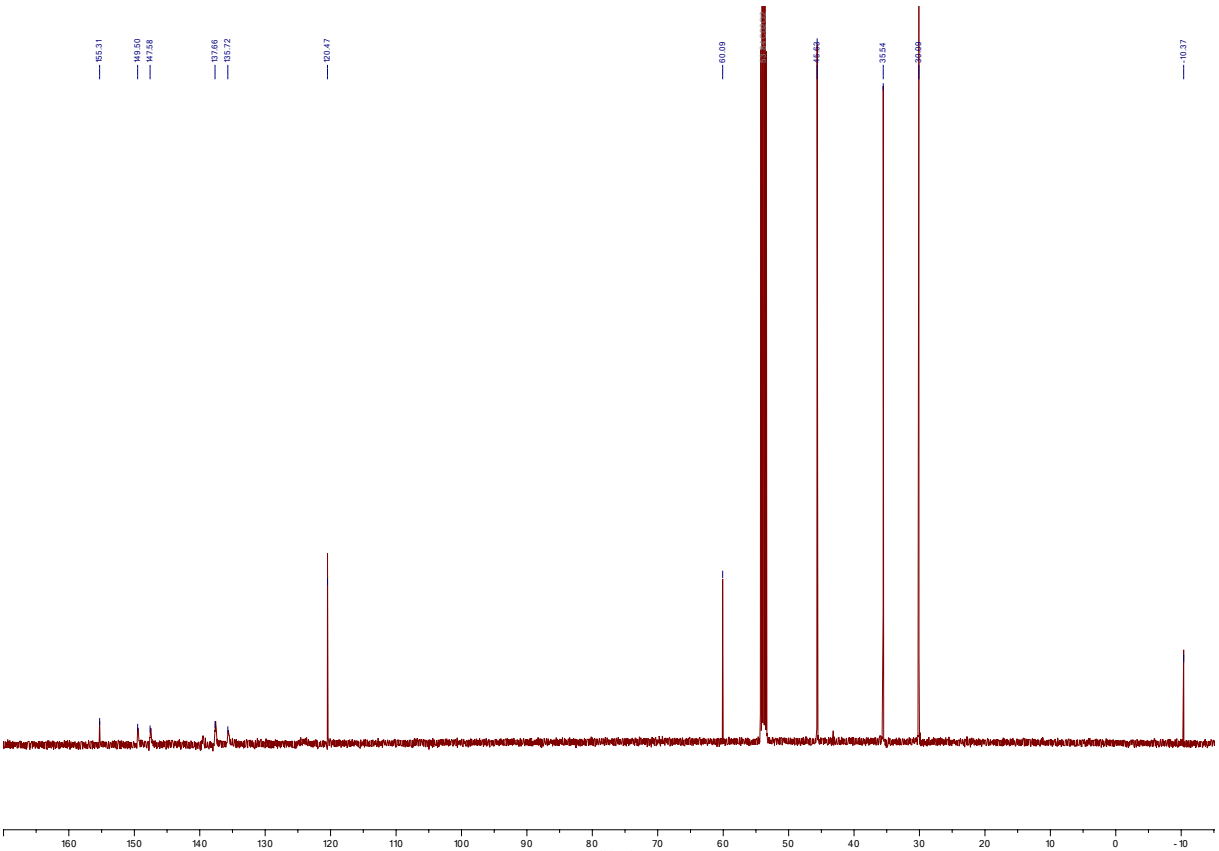

Figure S15. $^{13}C\{^{1}H\}$ NMR (125 MHz) of [IAdZnMe][$B(C_6F_5)_4$] ([**7**][$B(C_6F_5)_4$]) in CD_2Cl_2.

Figure S16. 2D HSQC NMR (500 MHz) of [IAdZnMe][$B(C_6F_5)_4$] ([**7**][$B(C_6F_5)_4$]) in CD_2Cl_2.

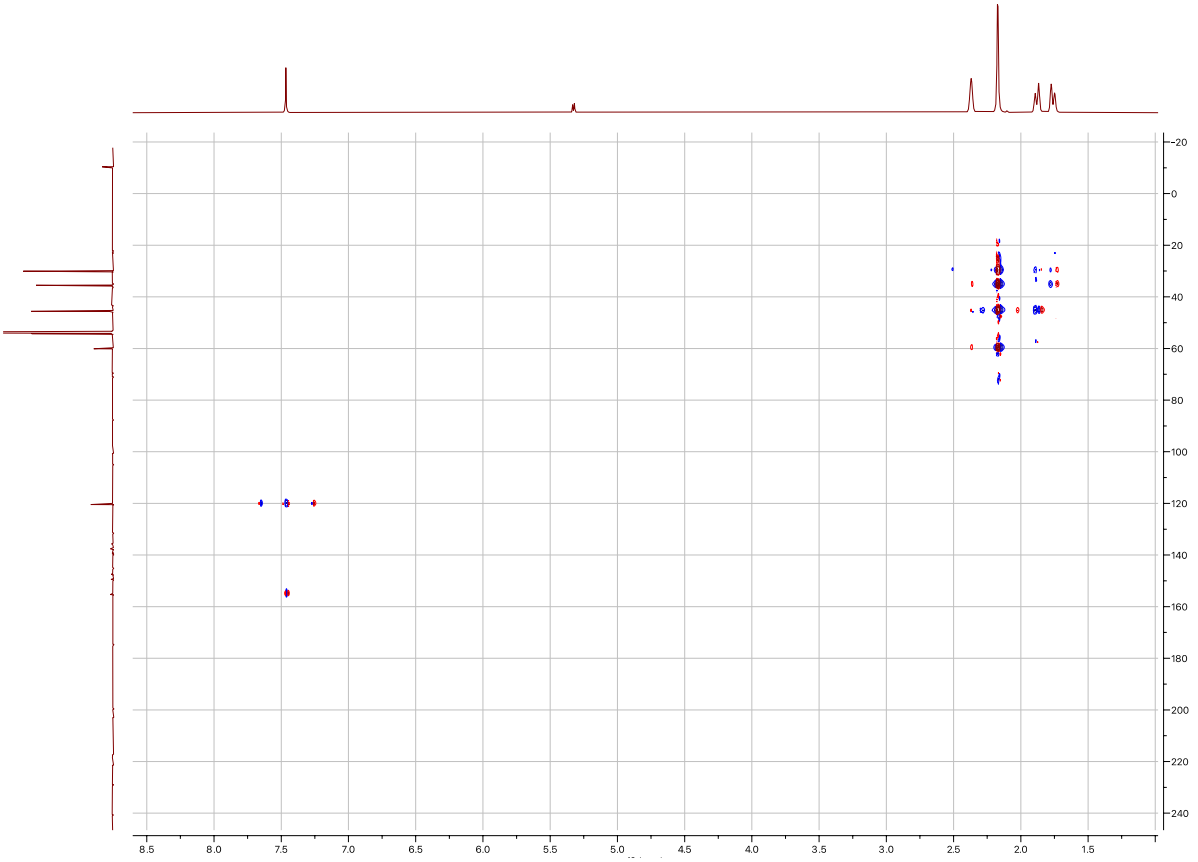

Figure S17. 2D HMBC NMR (500 MHz) of [IAdZnMe][$B(C_6F_5)_4$] ([**7**][$B(C_6F_5)_4$]) in CD_2Cl_2.

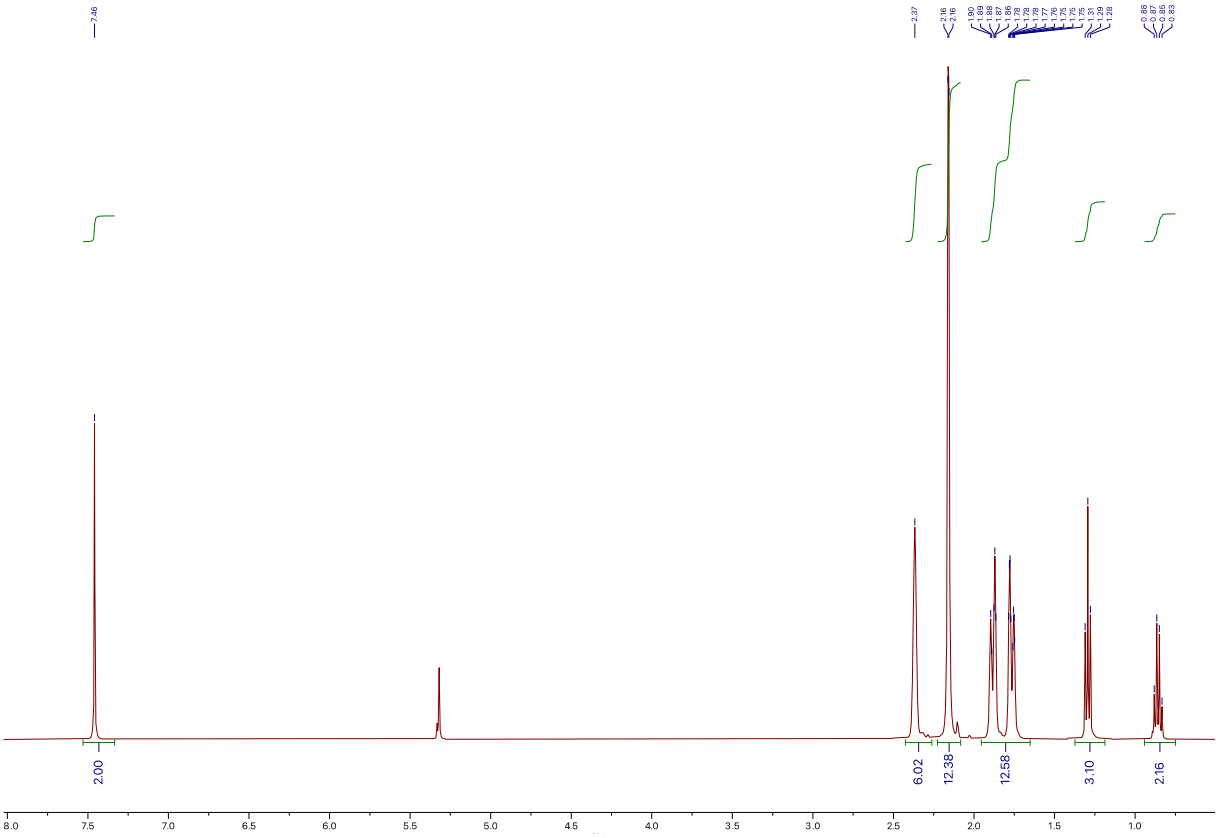

Figure S18. ^1H NMR (500 MHz) of [IAdZnEt][$B(C_6F_5)_4$] ([**8**][$B(C_6F_5)_4$]) in CD_2Cl_2.

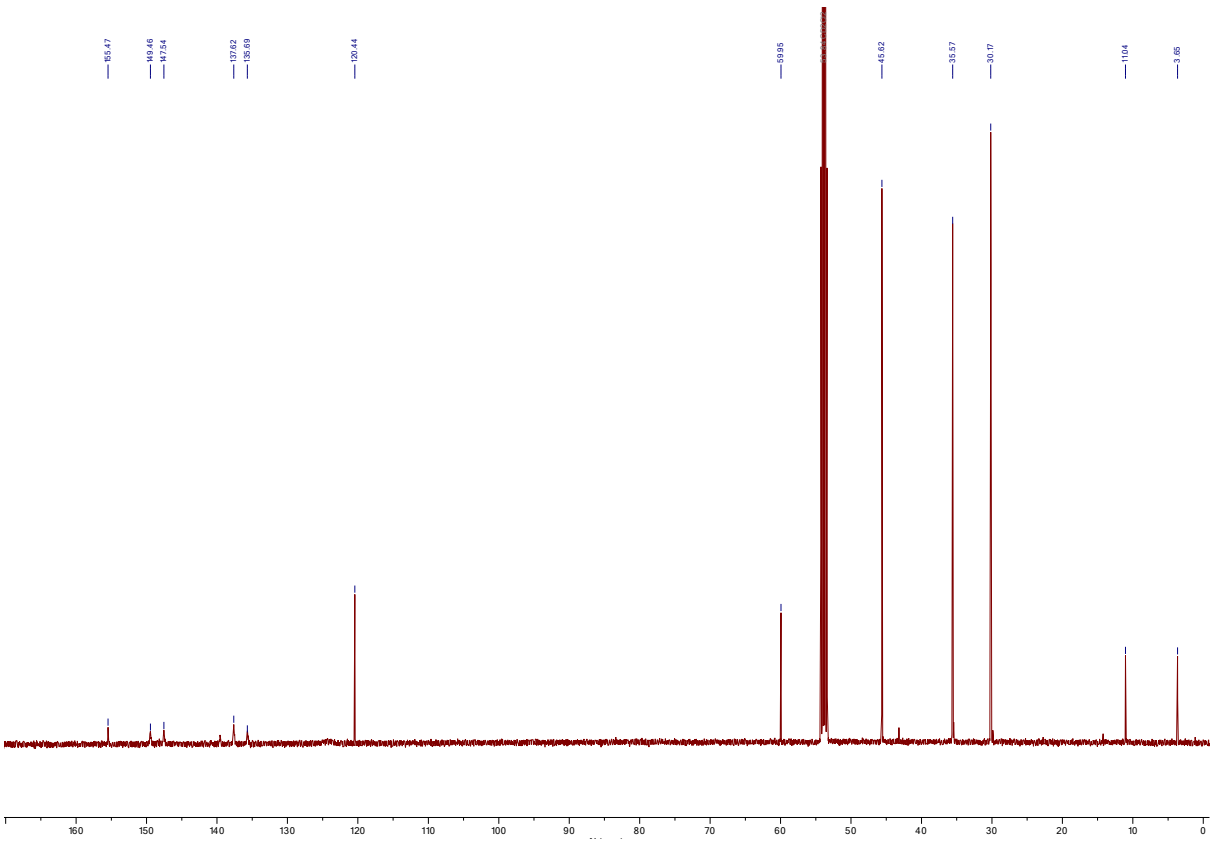

Figure S19. $^{13}C\{^{1}H\}$ NMR (125 MHz) of [IAdZnEt][$B(C_6F_5)_4$] ([**8**][$B(C_6F_5)_4$]) in CD_2Cl_2.

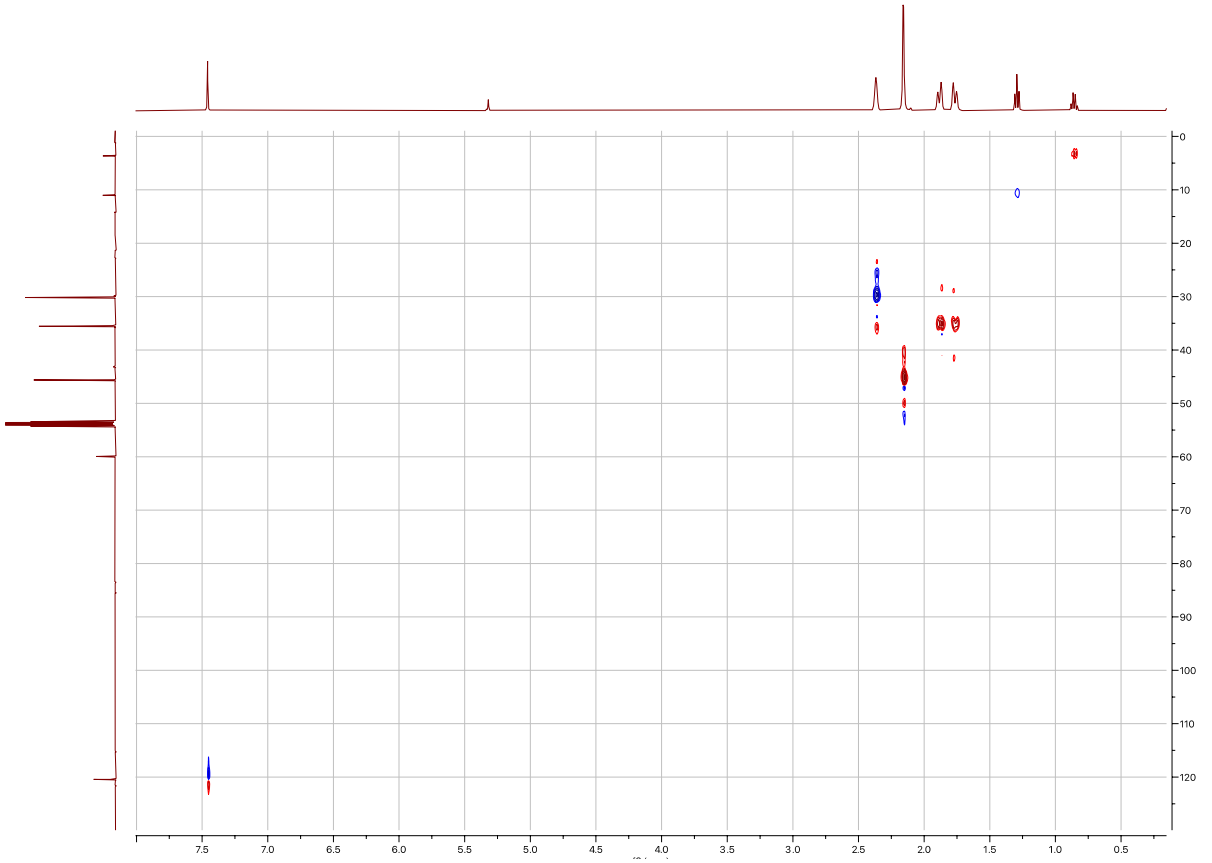

Figure S20. 2D HSQC NMR (500 MHz) of [IAdZnEt][$B(C_6F_5)_4$] ([**8**][$B(C_6F_5)_4$]) in CD_2Cl_2.

Figure S21. 2D HMBC NMR (500 MHz) of [IAdZnEt][$B(C_6F_5)_4$] ([**8**][$B(C_6F_5)_4$]) in CD_2Cl_2.

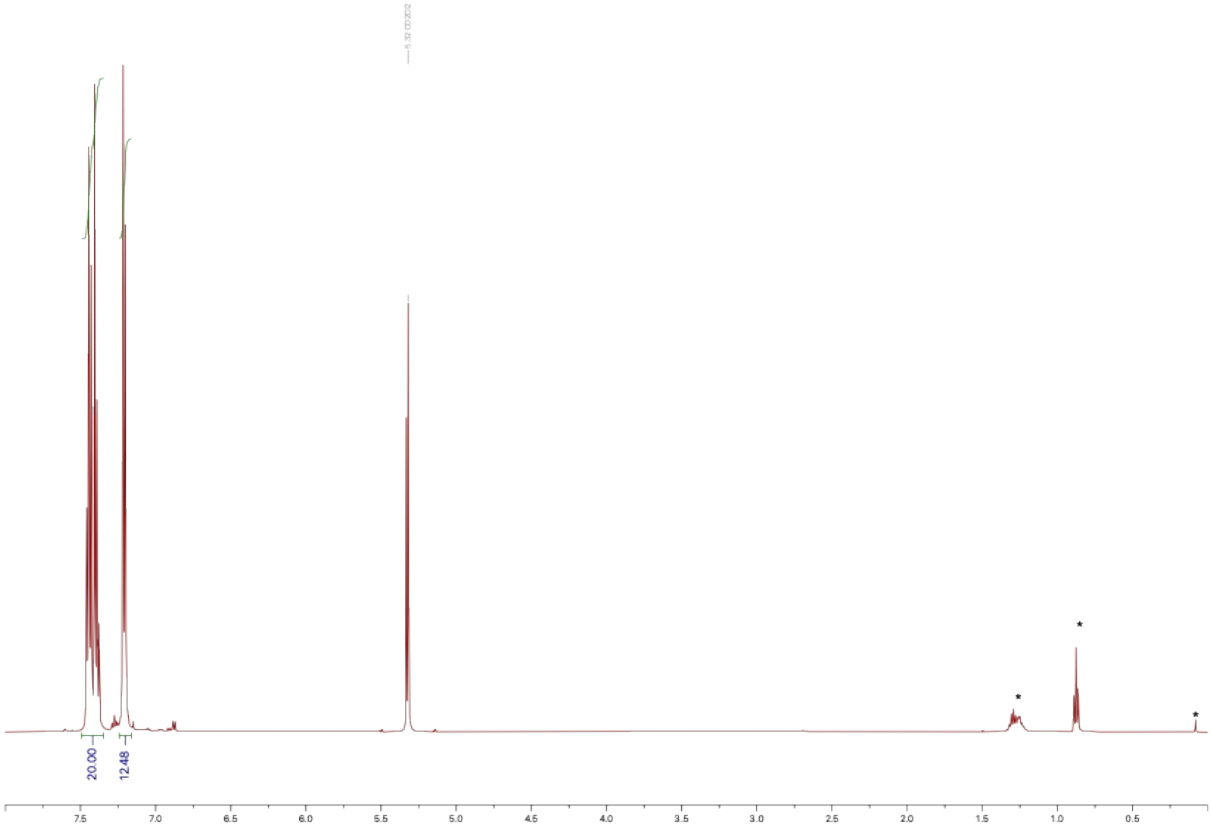

Figure S22. ^1H NMR (500 MHz) of [ITrZnC_6F_5][$B(C_6F_5)_4$] ([**9**][$B(C_6F_5)_4$]) in CD_2Cl_2 (*: residual pentane and grease peaks).

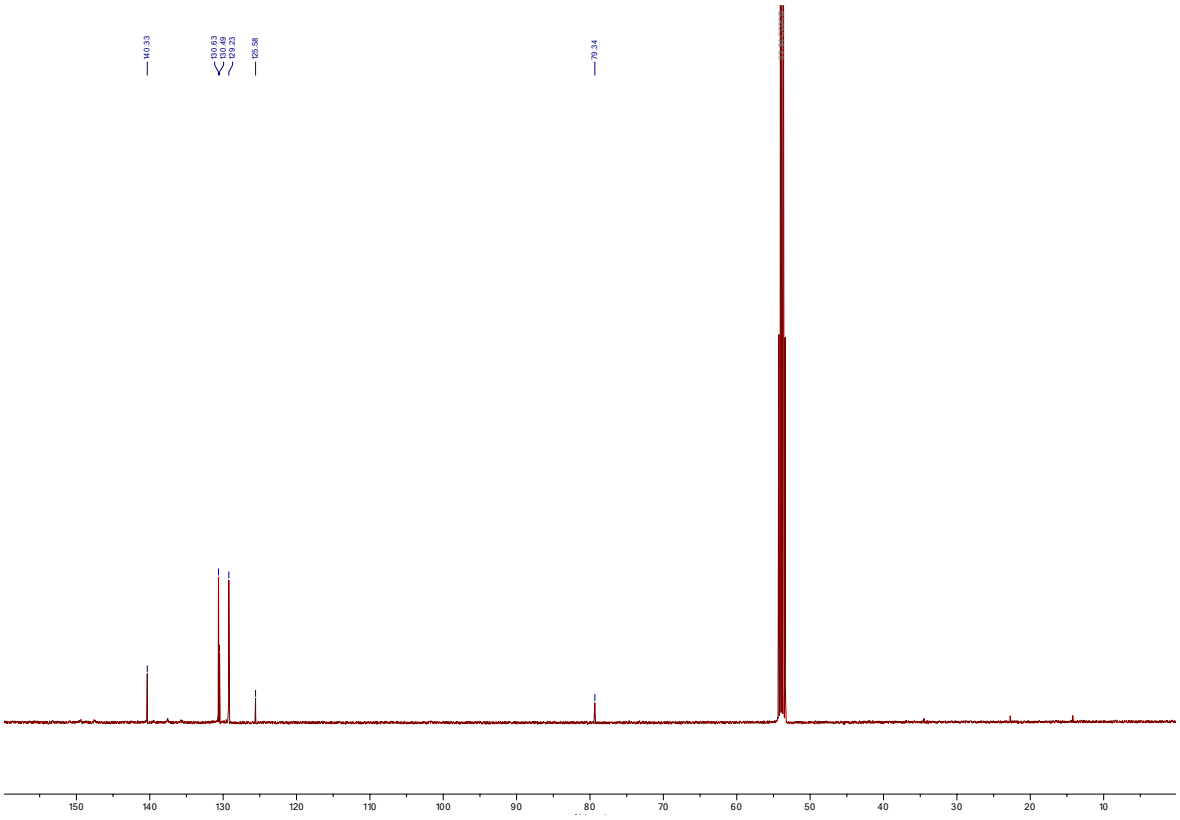

Figure S23. $^{13}C\{^{1}H\}$ NMR (125 MHz) of $[ITrZnC_6F_5][B(C_6F_5)_4]$ ([**9**][$B(C_6F_5)_4$]) in CD_2Cl_2.

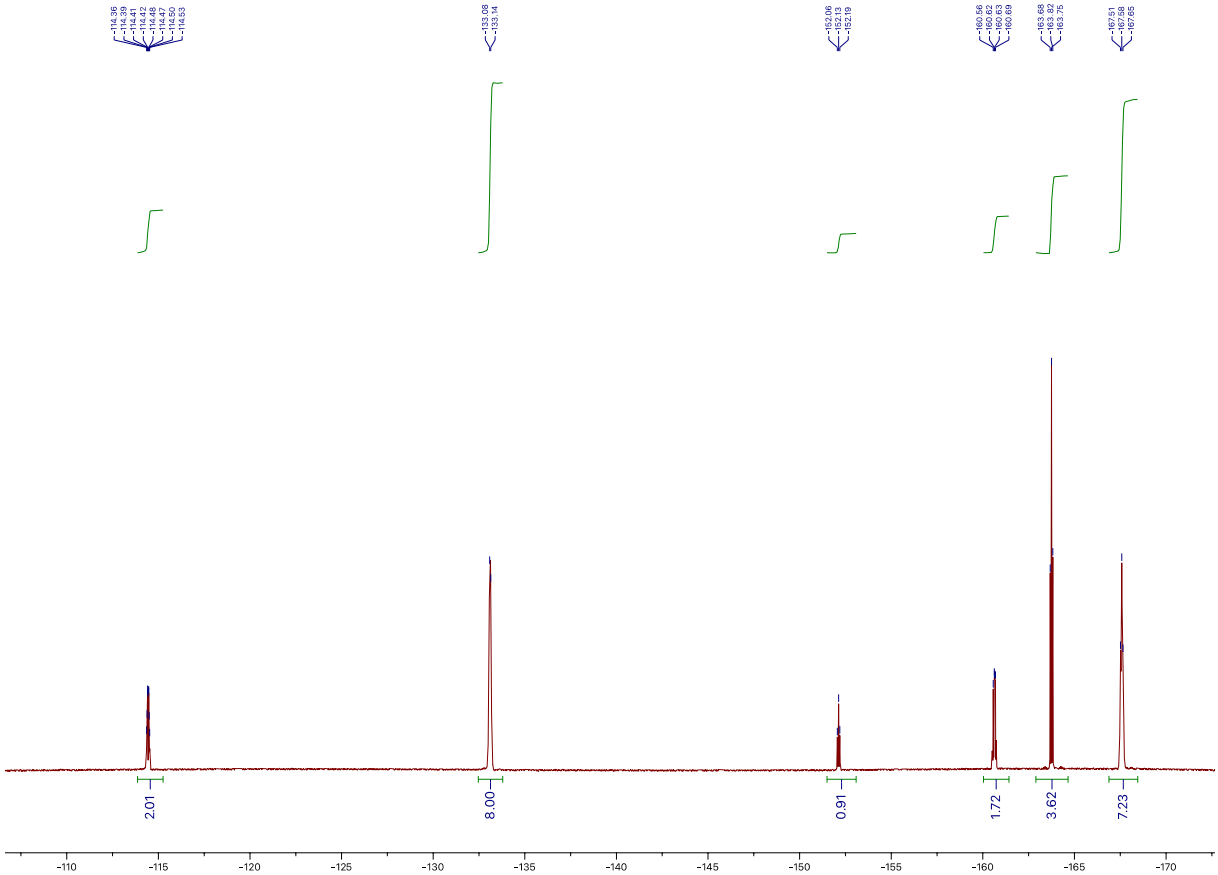

Figure S24. ^{19}F NMR (282 MHz) of $[ITrZnC_6F_5][B(C_6F_5)_4]$ ([**9**][$B(C_6F_5)_4$]) in CD_2Cl_2.

Crystallographic Details

X-Ray diffraction data collections for species **2**, [**5-6**][$B(C_6F_5)_4$], [**8**][$B(C_6F_5)_4$], [**9**][$B(C_6F_5)_4$] and [**11**][$B(C_6F_5)_4]_2$ were all carried out on a Bruker APEX II DUO Kappa-CCD diffractometer equipped with an Oxford Cryosystem liquid N_2 device, using Mo-Kα radiation (λ = 0.71073 Å). The crystal-detector distance was 38 mm. The cell parameters were determined (APEX2 software) from reflections taken from tree sets of 12 frames, each at 10s exposure. The structure was solved by direct methods using the program SHELXS-97. The refinement and all further calculations were carried out using SHELXL-97. The H atoms were included in calculated positions and treated as riding atoms using SHELXL default parameters. The non-H atoms were refined anisotropically, using weighted full-matrix least-squares on F^2. CCDC 2372716-2372720 and 2373743 provide the crystallographic data for **2**, [**5-6**][$B(C_6F_5)_4$], [**9**][$B(C_6F_5)_4$], [**11**][$B(C_6F_5)_4]_2$, and [**8**][$B(C_6F_5)_4$] respectively.

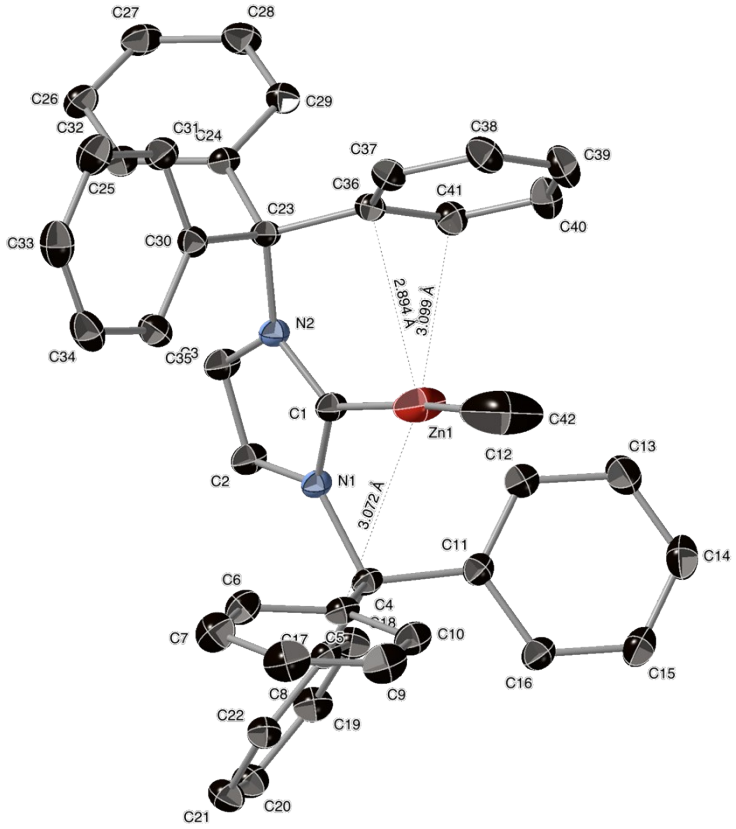

Figure S25. Molecular structure (ORTEP view) of Zn cation [(ITrZnMe]$^+$ ([**5**]$^+$). Selected bond distances (Å) and angles (°). Zn1-C1 = 1.966(1), C1-N1 = 1.352(2), C1-N2 = 1.352(1), Zn1-C42 = 1.914(2), C42-Zn1-C1 = 175.54(9).

NMR data on the reactivity of $[ITrZnC_6F_5][B(C_6F_5)_4]$ ($[\mathbf{9}][B(C_6F_5)_4]$) with H_2O

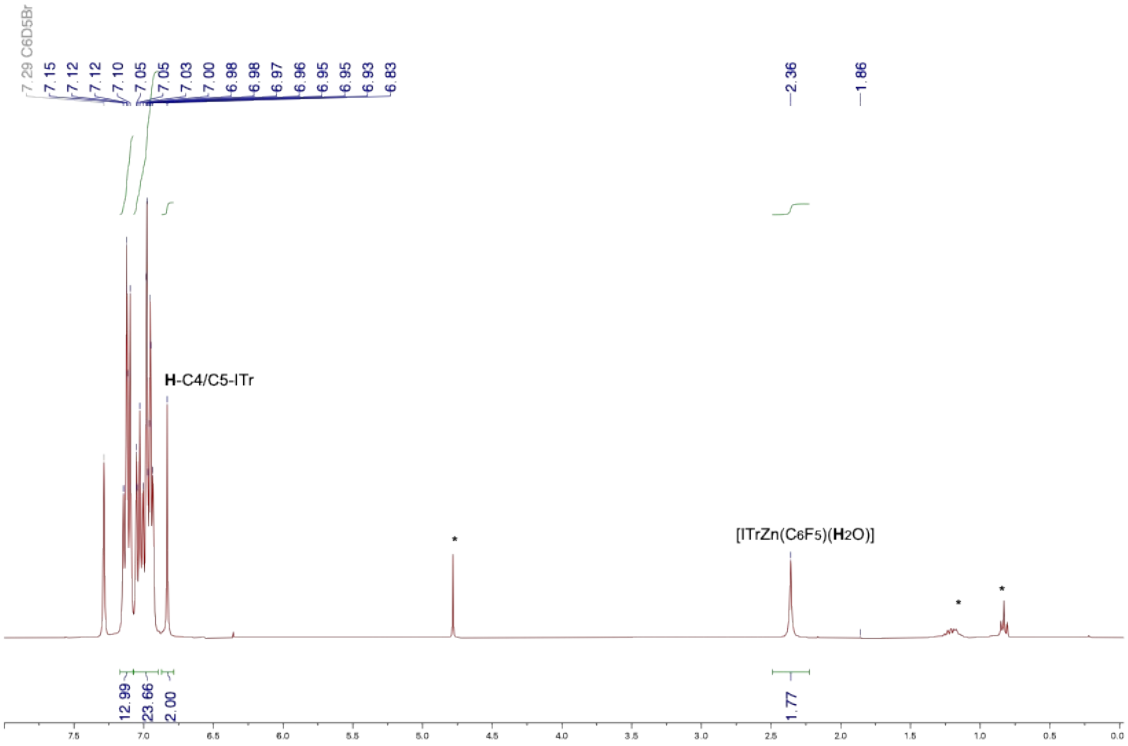

Figure S26. ^{1}H NMR (500 MHz) of the reaction of $[ITrZnC_6F_5][B(C_6F_5)_4]$ ($[\mathbf{9}][B(C_6F_5)_4]$) in C_6D_5Br after 15 min at RT, consistent with the formation of the Zn-OH_2 adduct $[ITrZn(C_6F_5)(OH_2)][B(C_6F_5)_4]$ ($[\mathbf{10}][B(C_6F_5)_4]$). Overlap with the signals of residual C_6D_4HBr (from the NMR solvent) results in higher-than-expected integration in the aromatic region. *: residual pentane + CH_2Cl_2.

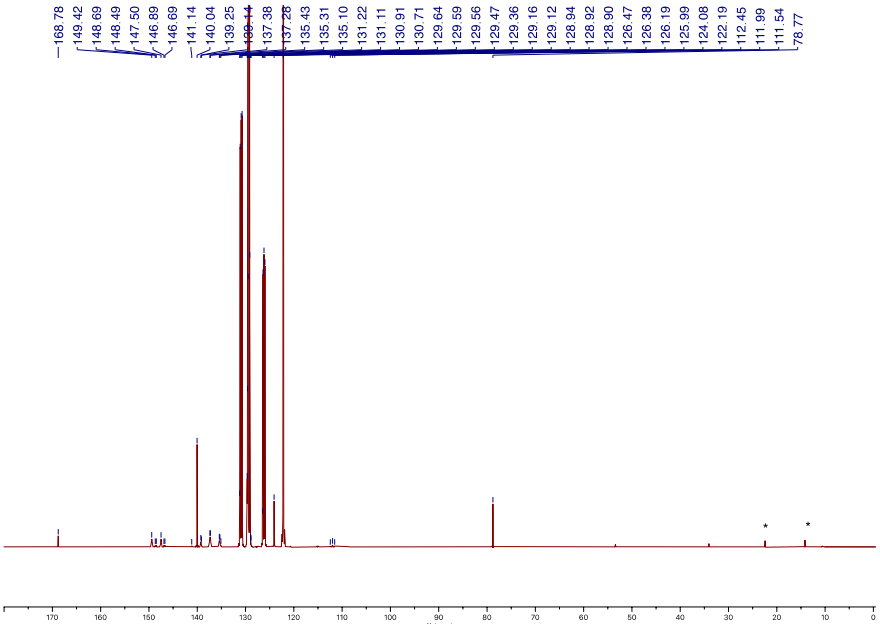

Figure S27. ^{13}C NMR (125 MHz) of *in situ* generated $[ITrZn(C_6F_5)(OH_2)][B(C_6F_5)_4]$ ($[\mathbf{10}][B(C_6F_5)_4]$) in C_6D_5Br. *: residual pentane.

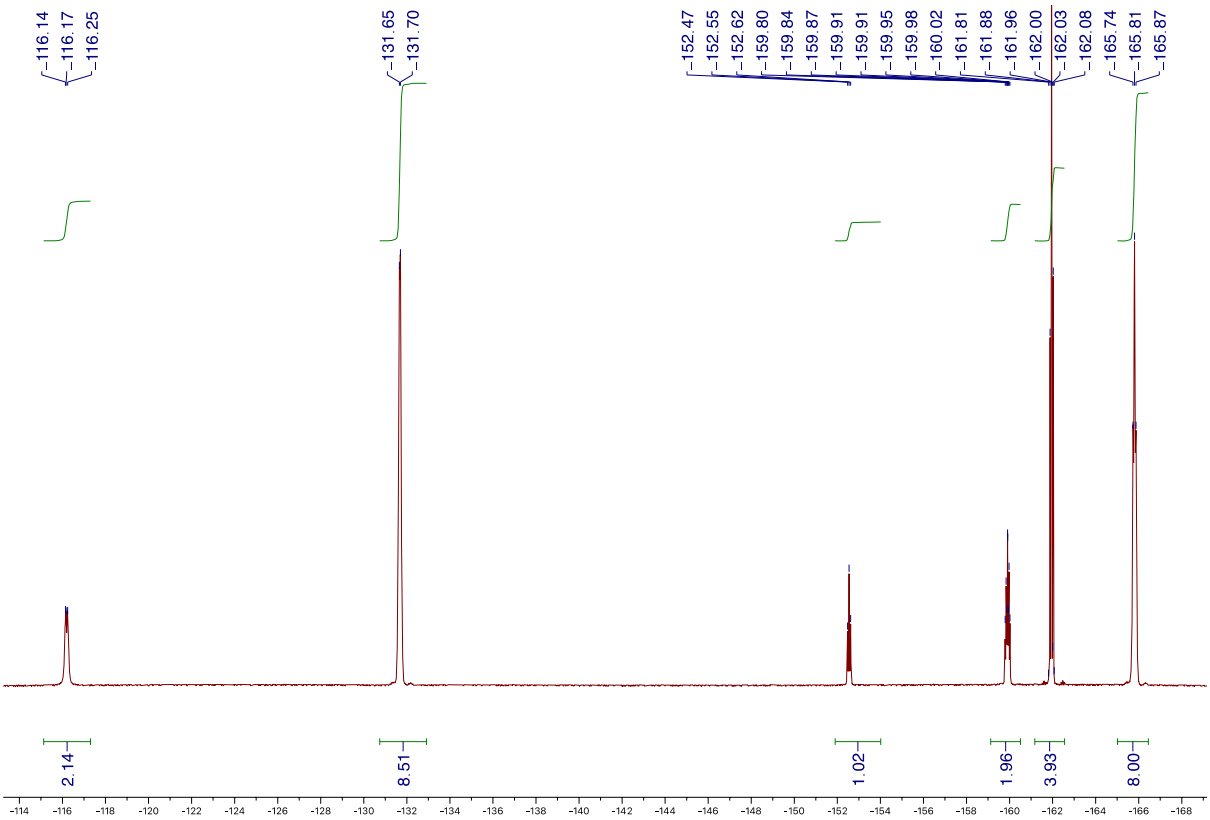

Figure S28. ^{19}F NMR (282 MHz) of *in situ* generated $[ITrZn(C_6F_5)(OH_2)][B(C_6F_5)_4]$ ([**10**][$B(C_6F_5)_4$]) in C_6D_5Br.

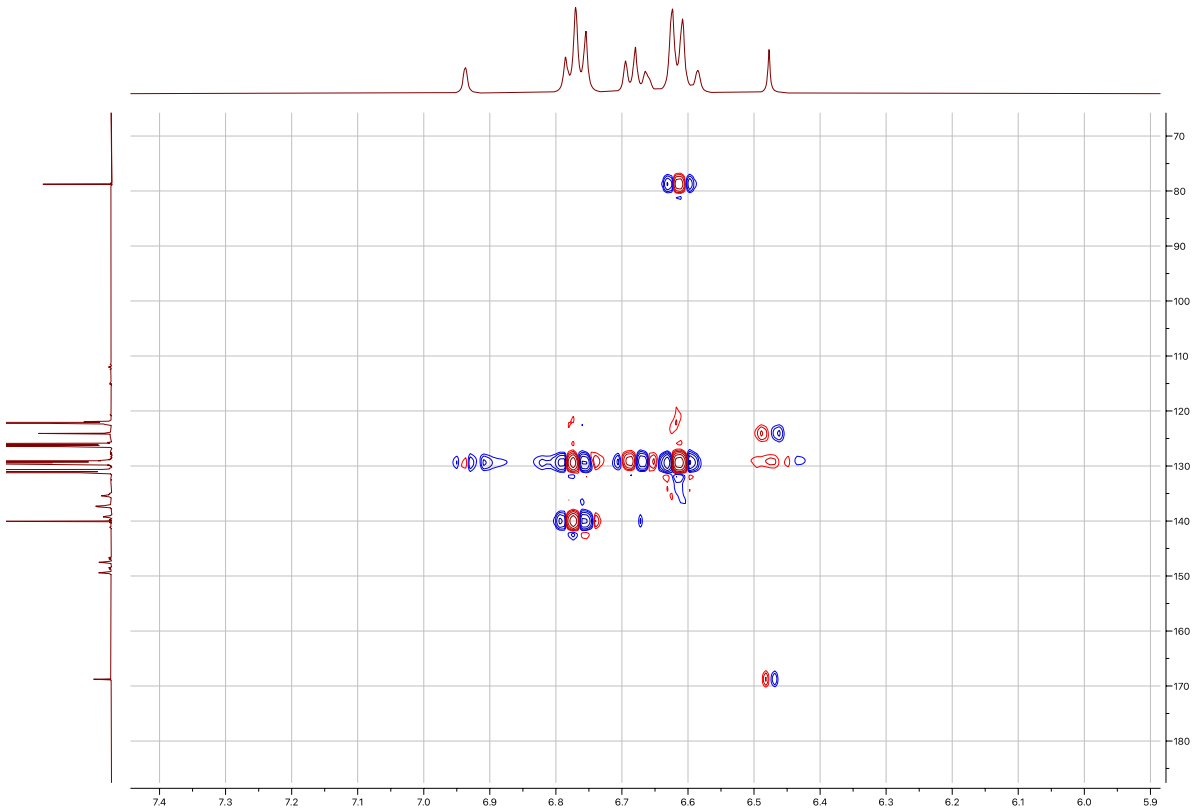

Figure S29. 2D HMBC NMR (500 MHz) of *in situ* generated $[ITrZn(C_6F_5)(OH_2)][B(C_6F_5)_4]$ ([**10**][$B(C_6F_5)_4$]) in C_6D_5Br.

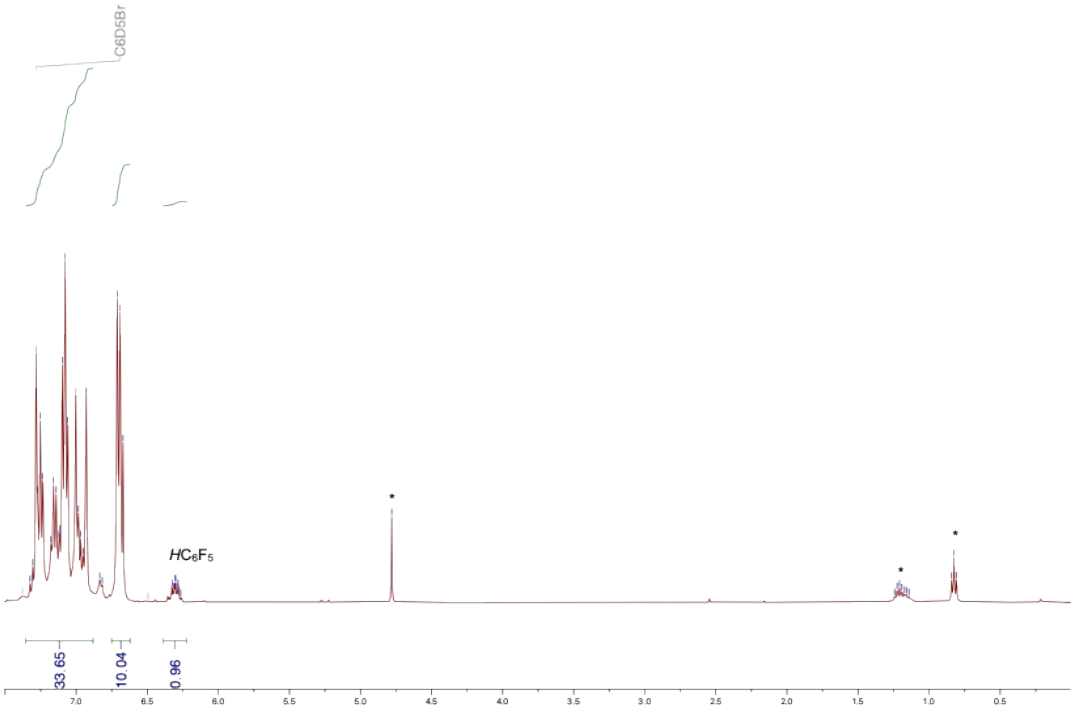

Figure S30. ^{1}H NMR (500 MHz) of [ITrZn(C_6F_5)(OH_2)][B(C_6F_5)$_4$] ([**10**][B(C_6F_5)$_4$]) in C_6D_5Br (with an initial concentration of 0.044 M) after 24 h at 60 °C showing substantial hydrolysis with the formation of C_6F_5H. Overlap with the signals of residual C_6D_4HBr (from the NMR solvent) results in higher-than-expected integration in the aromatic region. *: residual pentane + CH_2Cl_2.

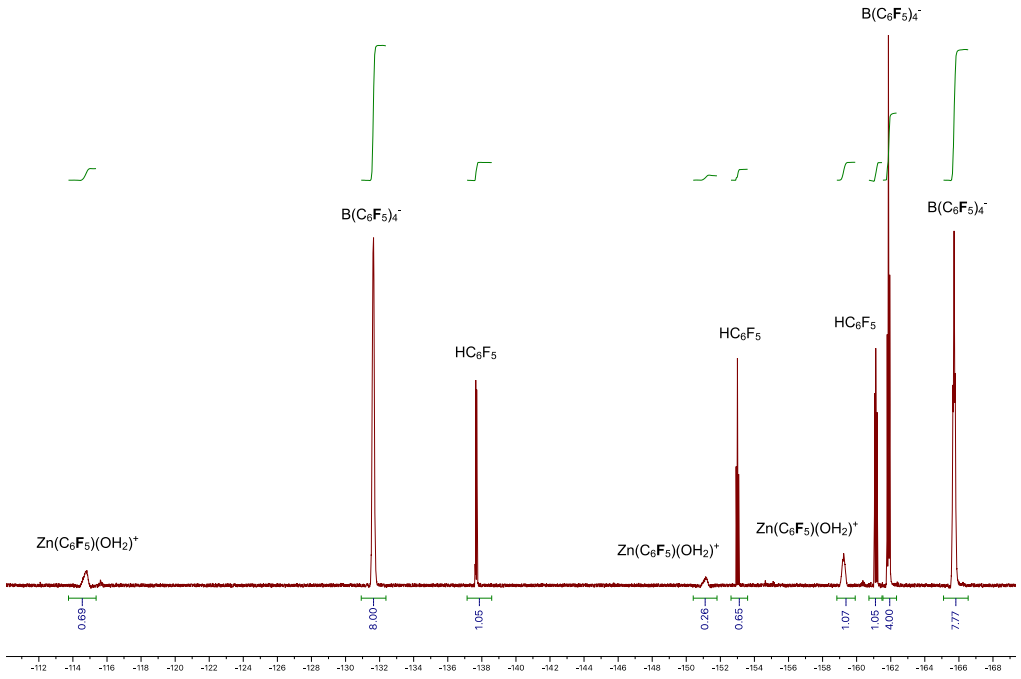

Figure S31. ^{19}F NMR (282 MHz) of [ITrZn(C_6F_5)(OH_2)][B(C_6F_5)$_4$] ([**10**][B(C_6F_5)$_4$]) in C_6D_5Br (with an initial concentration of 0.044 M) after 24 h at 60 °C leading to a 1/1 C_6F_5H/[**10**][B(C_6F_5)$_4$] mixture, in line with a 50% hydrolysis of the Zn-C_6F_5 bond of the starting [**10**][B(C_6F_5)$_4$].

NMR data for the catalysis runs

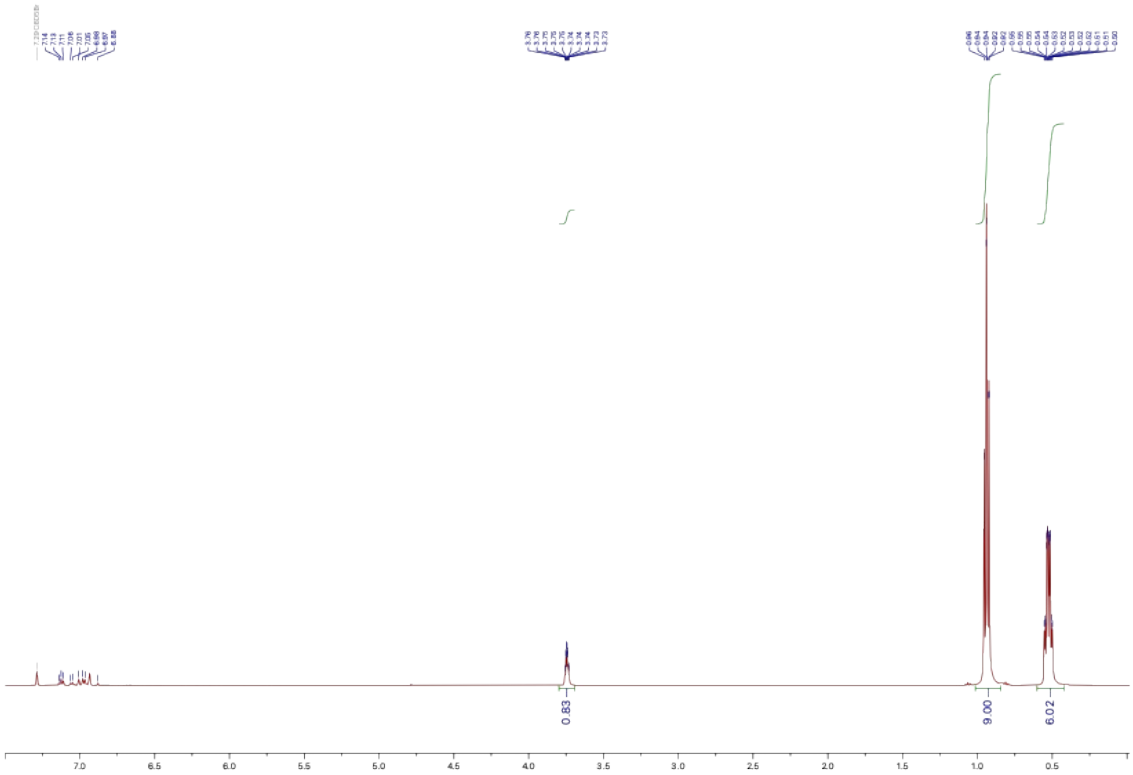

Figure S32. ^{1}H NMR (500 MHz, C_6D_5Br) of CO_2 (1.5 bar) hydrosilylation catalysis with $HSiEt_3$ using [**10**][$B(C_6F_5)_4$] (5% mol) as catalyst after 1 h at room temperature showing the absence of any reaction.

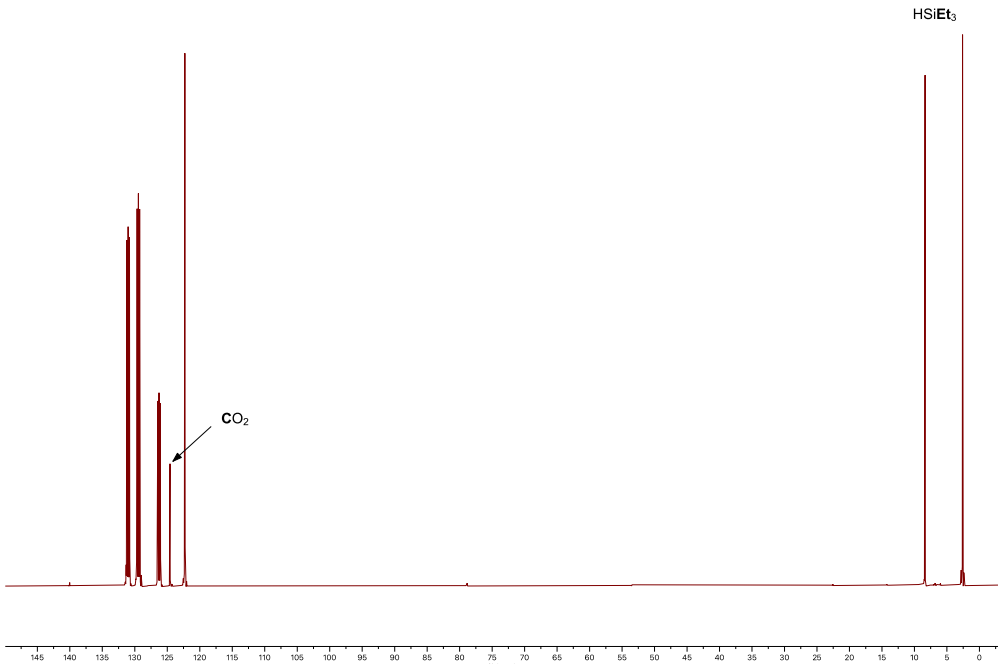

Figure S33. $^{13}C\{^{1}H\}$ NMR (500 MHz, C_6D_5Br) of CO_2 (1.5 bar) hydrosilylation catalysis with $HSiEt_3$ using [**10**][$B(C_6F_5)_4$] (5% mol) as catalyst after 1 h at room temperature showing the absence of any reaction.

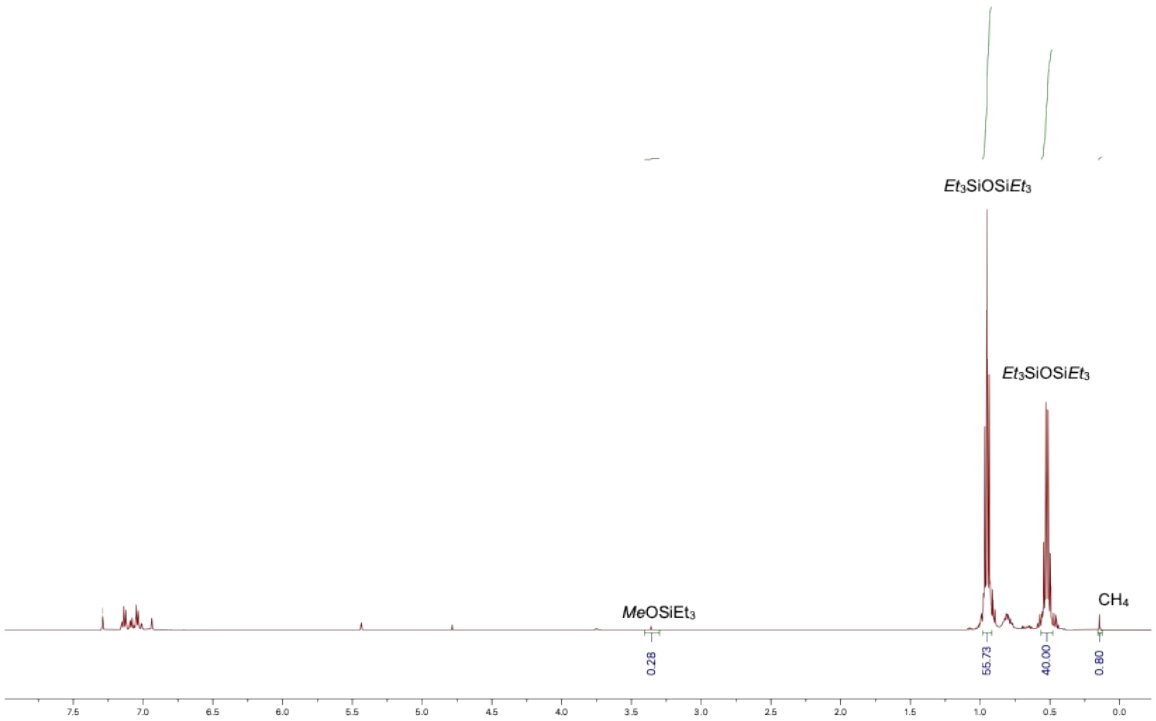

Figure S34. ^{1}H NMR (500 MHz, C_6D_5Br) of CO_2 (1.5 bar) hydrosilylation catalysis with $HSiEt_3$ using [**10**][$B(C_6F_5)_4$] (5% mol) as catalyst after 18 h at 90 °C showing complete $HSiEt_3$ conversion to a 95/5 CH_4/$MeOSiEt_3$ mixture along with $Et_3SiOSiEt_3$ as side product.

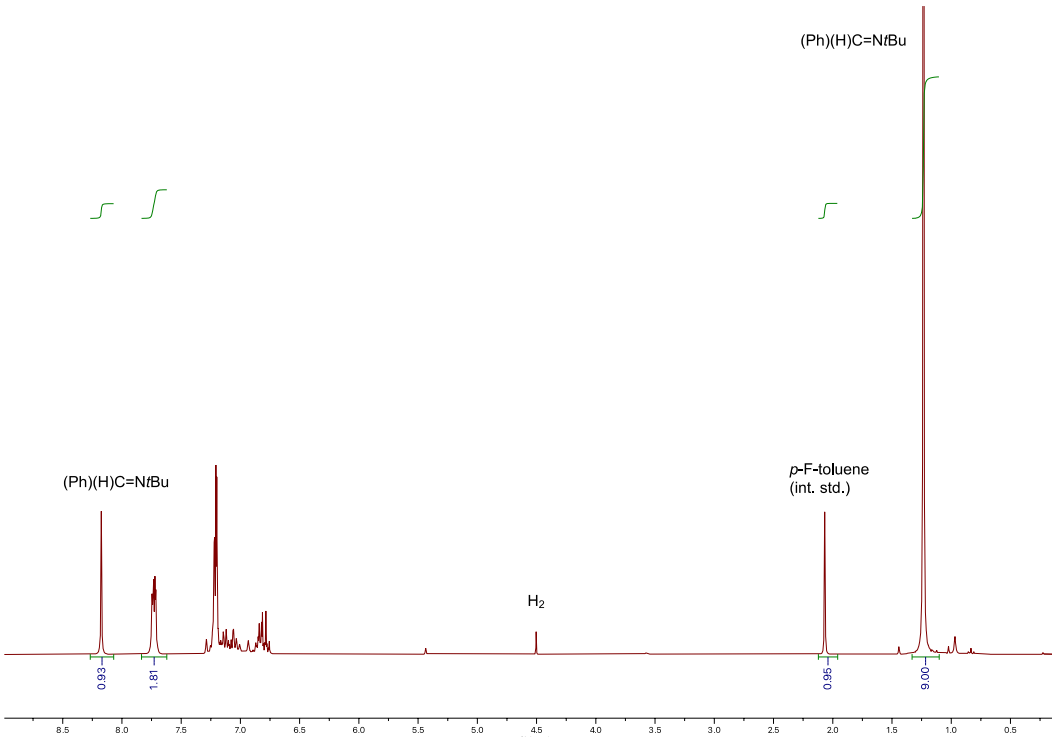

Figure S35. ^{1}H NMR (500 MHz, C_6D_5Br) of catalytic hydrogenation of imine PhCH=N*t*Bu in the presence of H_2 (2 bar) using [**10**][$B(C_6F_5)_4$] (5% mol) as catalyst after 1 h at room temperature showing the absence of any reaction.

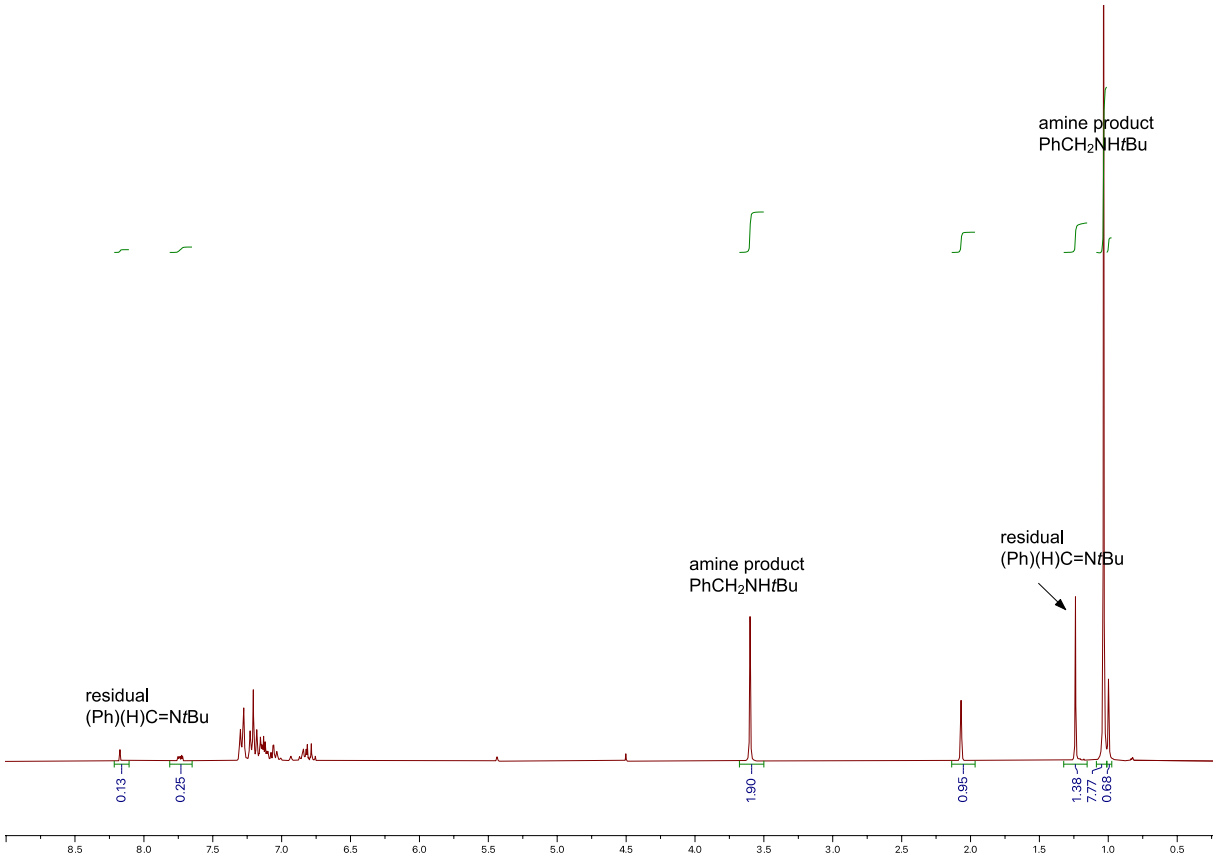

Figure S36. ^{1}H NMR (500 MHz, C_6D_5Br) of catalytic hydrogenation of imine PhCH=N*t*Bu in the presence of H_2 (2 bar) using [**10**][$B(C_6F_5)_4$] (5% mol) as catalyst after 24 h at 90 °C showing showing 90% conversion of the starting imine to the corresponding amine product $PhCH_2NHtBu$.

DFT calculations

All calculations have been performed with GAUSSIAN 09 version D01[1] at DFT level of theory with ωB97XD functional.[2] All atoms were described by 6-31+G** basis set.[3] All energies were estimated in the gas phase except the bonding free energy of ITr with $ZnEt_2$ computed in PhBr by mean of a PCM.[4] All structures were fully optimized, and the nature of the encountered stationary point determined by frequency analysis. Energy minima were characterized by a full set of real frequencies and transition states by one imaginary frequency. Gibbs Free energies were extracted from this frequency analysis. Non- Covalent Interaction analysis were performed on the GAUSSIAN wavefuntion of the optimized structures using NCIPLOT package using default parameters.[5]

Lewis acidity assessment through DFT-calculated Fluoride Ion Affinity (FIA).[6]

FIAs of cations were estimated in PhBr by DFT calculating the reaction enthalpy of each considered Lewis acid with the fluoride anion (see equation below and Table S1). All calculations have been performed with GAUSSIAN 09 version D01[1] at DFT level of theory with wB97XD functional.[2] All atoms were described by 6-31+G** basis set.[3] For comparison with the studied Zn cations, the FIA for the Zn cation $[(IPr)Zn–C_6F_5]^+$ is also included in Table S1.[7]

$[C] + F^- \rightarrow [C(F)]^-$ C = Lewis acid

Table S1. Fluoride Ion Affinity (FIA, gas phase) as estimated by DFT

	kJ/mol
$(ITr)Zn–Et^+$	102.1
$(IAd)Zn–Et^+$	129.7
$(ITr)Zn–C_6F_5^+$	118.5
$(IPr)Zn–C_6F_5^+$	156

Estimation of the pKa of the water adduct [(ITr)Zn(C_6F_5)(OH_2)][$B(C_6F_5)_4$] ([10][$B(C_6F_5)_4$])

The pKa of cation [(ITr)Zn(C_6F_5)(OH_2)]$^+$ ([**10**]$^+$) was estimated in MeCN using the relative method.[8] In this method, the pKa of the acid (here [**10**]$^+$) here is expressed by the acidity of another acid, for which the experimental pKa is known (an isodesmic reaction). In the present case, pyridinium was used as the other acid since its pKa in MeCN is well-established (pKa = 12.53).[8,9] The Gibbs free enthalpy of the reaction of [**10**]$^+$ and pyridine to yield the corresponding Zn-OH and pyridinium was then DFT-estimated in MeCN (eq. 1 below). The reaction is endergonic with ΔG = 11.5 kcal.mol^{-1} leading to an equilibrium constant of $10^{-8.43}$ (*K*).

(1) 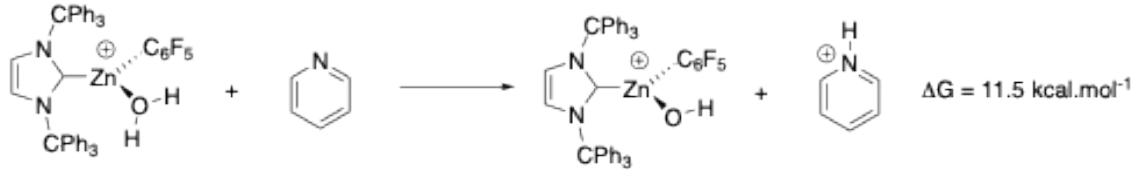

Given that $K = Ka_{[\mathbf{10}]+}/Ka_{[pyH]+}$, it follows that $Ka_{[\mathbf{10}]+} = K \times Ka_{[pyH]+} = 10^{-8.43} \times 10^{-12.53} = 10^{-20.96}$.

The *K*a is cation [**10**]$^+$ is thus estimated to be around 21, albeit within the limit of validity of the method. In this regard, given the limitations of the PCM to estimate solvation energies, we also estimated the Gibbs free energy (in MeCN) of the reaction of pyridine + H_2O to yield pyridinium and [OH]$^-$ (eq. 2 below), and compared our results to known experimental estimations to validate our approach.

(2) 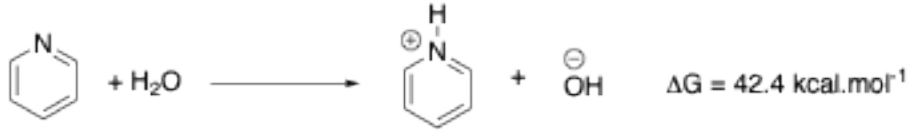

The above reaction is highly endergonic, with ΔG = 42.4 kcal.mol^{-1} leading to an equilibrium constant of $K' = 10^{-31.1}$. Given that $K' = Ka_{H2O}/Ka_{[pyH]+}$, it can also be estimated from experimental data: the pKa of H_2O in MeCN ≈ 38-41,[10] and that of pyridinium is 12.53. This leads to a rough estimate of p*K'* between 25.5 and 28.5 (*vs.* 31.1 from DFT calculations), which is reasonable given the limitations of PCM as well as experimental uncertainties.

References

(1) M. J. Frisch, G. W. Trucks, H. B. Schlegel, G. E. Scuseria, M. A. Robb, J. R. Cheeseman, G. Scalmani, V.Barone, B. Mennucci, G. A. Petersson, H. Nakatsuji, M. Caricato, X. Li, H. P. Hratchian, A. F. Izmaylov, J. Bloino, G. Zheng, J. L. Sonnenberg, M. Hada, M. Ehara, K. Toyota, R. Fukuda, J. Hasegawa, M. Ishida, T. Nakajima, Y. Honda, O. Kitao, H. Nakai, T. Vreven, J. A. Montgomery, Jr., J. E. Peralta, F. Ogliaro, M. Bearpark, J. J. Heyd, E. Brothers, K. N. Kudin, V. N. Staroverov, R. Kobayashi, J. Normand, K. Raghavachari, A. Rendell, J. C. Burant, S. S. Iyengar, J. Tomasi, M. Cossi, N. Rega, J. M. Millam, M. Klene, J. E. Knox, J. B. Cross, V. Bakken, C. Adamo, J. Jaramillo, R. Gomperts, R. E. Stratmann, O. Yazyev, A. J. Austin, R. Cammi, C. Pomelli, J. W. Ochterski, R. L. Martin, K. Morokuma, V. G. Zakrzewski, G. A. Voth, P. Salvador, J. J. Dannenberg, S. Dapprich, A. D. Daniels, Ö. Farkas, J. B. Foresman, J. V. Ortiz, J. Cioslowski, D. J. Fox. Gaussian 09 Revision A.2. Gaussian Inc. Wallingford CT 2009.

(2) Chai, J.-D.; Head-Gordon, M. Long-Range Corrected Hybrid Density Functionals with Damped Atom–Atom Dispersion Corrections. *Phys. Chem. Chem. Phys.* **2008**, *10* (44), 6615. https://doi.org/10.1039/b810189b.

(3) Ditchfield, R.; Hehre, W. J.; Pople, J. A. Self-Consistent Molecular-Orbital Methods. IX. An Extended Gaussian-Type Basis for Molecular-Orbital Studies of Organic Molecules. *J. Chem. Phys.* **2003**, *54* (2), 724–728. https://doi.org/10.1063/1.1674902.

(4) Miertuš, S.; Scrocco, E.; Tomasi, J. Electrostatic Interaction of a Solute with a Continuum. A Direct Utilizaion of AB Initio Molecular Potentials for the Prevision of Solvent Effects. *Chem. Phys.* **1981**, *55* (1), 117–129. https://doi.org/10.1016/0301-0104(81)85090-2.

(5) Contreras-García, J.; Johnson, E. R.; Keinan, S.; Chaudret, R.; Piquemal, J.-P.; Beratan, D. N.; Yang, W. NCIPLOT: A Program for Plotting Noncovalent Interaction Regions. *J. Chem. Theory Comput.* **2011**, *7* (3), 625–632. https://doi.org/10.1021/ct100641a.

(6) Adet, N.; Specklin, D.; Gourlaouen, C.; Damiens, T.; Jacques, B.; Wehmschulte, R. J.; Dagorne, S. Towards Naked Zinc(II) in the Condensed Phase: A Highly Lewis Acidic ZnII Dication Stabilized by Weakly Coordinating Carborate Anions. *Angew. Chem. Int. Ed.* **2021**, *60* (4), 2084–2088. https://doi.org/10.1002/anie.202012287.

(7) Specklin, D.; Hild, F.; Fliedel, C.; Gourlaouen, C.; Veiros, L. F.; Dagorne, S. Accessing Two-Coordinate ZnII Organocations by NHC Coordination: Synthesis, Structure, and Use as π-Lewis Acids in Alkene, Alkyne, and CO2 Hydrosilylation. *Chem. – Eur. J.* **2017**, *23* (63), 15908–15912. https://doi.org/10.1002/chem.201704382.

(8) Mech, P.; Bogunia, M.; Nowacki, A.; Makowski, M. Calculations of pKa Values of Selected Pyridinium and Its N-Oxide Ions in Water and Acetonitrile. *J. Phys. Chem. A* **2020**, *124* (3), 538–551. https://doi.org/10.1021/acs.jpca.9b10319.

(9) Kütt, A.; Tshepelevitsh, S.; Saame, J.; Lõkov, M.; Kaljurand, I.; Selberg, S.; Leito, I. Strengths of Acids in Acetonitrile. *Eur. J. Org. Chem.* **2021**, *2021* (9), 1407–1419. https://doi.org/10.1002/ejoc.202001649.

(10) Felton, G. A. N.; Vannucci, A. K.; Okumura, N.; Lockett, L. T.; Evans, D. H.; Glass, R. S.; Lichtenberger, D. L. Hydrogen Generation from Weak Acids: Electrochemical and Computational Studies in the [(H5-C5H5)Fe(CO)2]2 System. *Organometallics* **2008**, *27* (18), 4671–4679. https://doi.org/10.1021/om800366h.